frontiers in Earth Science

ORIGINAL RESEARCH
published: 19 December 2019
doi: 10.3389/feart.2019.00341

Magnetic Susceptibility Record in Paleozoic Succession (Rhenohercynian Massif, Northern Europe) – Disentangling Sea Level, Local and Diagenetic Impact on the Magnetic Records

Damien Pas[1,2], Anne-Christine Da Silva[2], Geoffrey Poulain[3], Simo Spassov[4] and Frédéric Boulvain[2]*

[1] Paleomagnetic Laboratory, Utrecht University, Utrecht, Netherlands, [2] Pétrologie Sédimentaire, Université de Liège, Liège, Belgium, [3] Geolys, Brussels, Belgium, [4] Geophysical Centre, Royal Meteorological Institute of Belgium, Brussels, Belgium

OPEN ACCESS

Edited by:
Kenneth Philip Kodama, Lehigh University, United States

Reviewed by:
Yong-Xiang Li, Nanjing University, China
Belén Oliva-Urcia, Autonomous University of Madrid, Spain

***Correspondence:**
Damien Pas
damienpas@gmail.com

Specialty section:
This article was submitted to Geomagnetism and Paleomagnetism, a section of the journal Frontiers in Earth Science

Received: *18 September 2019*
Accepted: *04 December 2019*
Published: *19 December 2019*

Citation:
Pas D, Da Silva A-C, Poulain G, Spassov S and Boulvain F (2019) Magnetic Susceptibility Record in Paleozoic Succession (Rhenohercynian Massif, Northern Europe) – Disentangling Sea Level, Local and Diagenetic Impact on the Magnetic Records. Front. Earth Sci. 7:341. doi: 10.3389/feart.2019.00341

This study uses an integrated approach, including sedimentology, geochemistry and hysteresis magnetic measurements on a million year Givetian sequence in the southern margin of the Ardennes carbonate platform (France) to test the reliability of magnetic susceptibility (χ) records as inter-regional correlation tools in remagnetized settings. Furthermore, we aim to better understand the N-S depositional variations and sea-level fluctuations in the Ardennes. Sedimentological analyses revealed a complex platform evolution displaying a variety of shallow- and off-reef paleoenvironmental rocks, which ultimately allowed us to improve the sedimentological model of this area and to constrain the main sea-level fluctuations within the southern margin of the Ardennes platform. Comparison of the χ curve of this succession with previously published time-equivalent records in the western margin of the platform indicates a clear correlation between the two areas, despite the distance between the locales, their different sedimentology background and the remagnetization affecting the entire region. In contrast, the comparison of these χ profiles from the Ardennes (SW Rhenohercynian Massif, Belgian and France) with coeval data from the Rheinisches Schiefergebirge (NE Rhenohercynian Massif, Germany) do not show obvious correlations. Therefore, it is inferred that syn-sedimentary autogenic processes (e.g., vicinity to landmasses, wave agitation), which operate at small spatial and temporal scales affected the χ signal and could cause the lack of correlation between χ profiles.

Keywords: Paleozoic, carbonate, remagnetization, paleoenvironment, magnetic minerals, hysteresis, sedimentology

INTRODUCTION

Magnetic susceptibility is a proxy that has been broadly used for paleoenvionmental and correlation purposes in ancient sedimentary records (Ellwood et al., 2001; Bábek et al., 2007; Whalen and Day, 2008; 2010; Hladil et al., 2011; Da Silva et al., 2013; Chadimova et al., 2015). Recent advances in the interpretation of the χ signal have clearly demonstrated the influence of sedimentary settings and post-depositional transformation such as diagenesis and metamorphism (Jackson, 1990; Elmore et al., 1993; Channell and McCabe, 1994; Zegers et al., 2003; Da Silva and Boulvain, 2012; Da Silva et al., 2013). To better understand the effect of these processes on the χ signal, Riquier et al. (2010) and Da Silva et al. (2013) conducted rock magnetic studies on numerous Devonian limestone sections from the NE Rhenohercynian Massif, Ardennes, France and Morocco. Despite the remagnetization highlighted in the NE Rhenohercynian Massif and Ardennes (Molina Garza and Zijderveld, 1996; Zwing et al., 2002, 2005; Zegers et al., 2003), Riquier et al. (2010) and Da Silva et al. (2013) demonstrated that the primary depositionally-induced χ signal was at least partly preserved and that it could be used for paleoenvironmental and paleoclimatic interpretations. Therefore, it is essential to test the origin of the magnetic signal through the combined use of geochemical, facies analyses and hysteresis measurements (Riquier et al., 2010; Da Silva et al., 2015) before applying χ as a paleoclimatic or correlation tool for sections at any scale.

The reconstruction of Paleozoic carbonate platforms is often challenging because of numerous limiting parameters such as complex structural geology, diagenesis, lack of outcrops, differential denudation, ancient reefal communities, etc. In the Ardennes (Northern France, Southern Belgium), major parts of the Givetian platform are buried in the subsurface of major synclines or eroded in the core of anticlines, and relevant outcrops only expose short sections of this extensive platform. For these reasons, the main evolutionary phases of the Givetian Ardennes platform through space and time remain difficult to delineate. In this study, multiple proxies, such as sedimentology, geochemistry and hysteresis magnetic measurements are generated from the million year Fromelennes-Flohimont section in France (southern margin of the Ardennes platform). These data are then integrated with previously published data from the northern margin of the Ardennes platform [La Thure (LT) section] which include facies, geochemistry (Pas et al., 2017) and magnetic susceptibility analyses (De Vleeschouwer et al., 2015). This synthesis sheds new light on the depositional environments, their variations across the platform and the main sea-level fluctuations from the earliest to the latest Givetian time. To test the extent that magnetic susceptibility can be used for inter-regional correlations, we assessed the preservation of the paleoenvironmental information in the magnetic susceptibility records for the Fromelennes-Flohimont section through comparison with facies evolution, geochemical and magnetic hysteresis measurements. To further test the preservation of χ in the LT section (Pas et al., 2017), we also measure hysteresis on selected samples that is compared with published geochemical and magnetic susceptibility results (De Vleeschouwer et al., 2015; Pas et al., 2017). The χ record from the Fromelennes-Flohimont section is then compared with time equivalent published records in the Belgian LT and the German Burgberg sections.

GEOLOGICAL SETTING

This work focuses on the Fromelennes-Flohimont (FF) section, a Givetian (Middle Devonian) carbonate succession from the Ardennes Basin, located in northern France (50°07′04″, N 4°51′26″E, **Figure 1A**). In this study the FF section is compared with the LT section which is located in western Belgium (50°17′11″N, 4°09′40″E, Pas et al., 2017) and to the Burgberg section in Germany (51°24′47″N, 8°42′31″E; Pas et al., 2013). The FF and LT χ datasets were published as part of a Givetian cyclostratigraphic analysis by De Vleeschouwer et al. (2015). Later, the LT section was further investigated for an integrated multi-proxy sedimentological analysis (Pas et al., 2017). In Belgium, Givetian sediments crop out along the border of the Dinant and Vesdre Synclines, in the Philippeville Anticline and along the southern border of the Brabant Massif, within the Brabant Para-Autochthonous area and the Haine-Sambre-Meuse Overturned Thrust sheets (for precise location of these sheets, see Figure 5 in Belanger et al., 2012), which are all large-scale units of the Rhenohercynian fold-and-thrust belt (**Figure 1B**). This major tectonic structure formed during the Carboniferous to Permian as a consequence of the collision between the Laurussia and Gondwana supercontinents during the Variscan orogeny. The tectonic shortening of the pre-Mesozoic sequences in the Rhenohercynian Zone associated with this collision is estimated at ∼40% (Dittmar et al., 1994). Therefore, considering the present day distance of ∼50 km separating the FF from the LT section, we assume a distance of ∼85 km between these two sites at the time of deposition.

Several authors provided evidence that during this orogeny, the rocks belonging to the Rhenohercynian fold-and-thrust belt were affected by remagnetization (e.g., Molina Garza and Zijderveld, 1996; Zegers et al., 2003; Zwing et al., 2005; Da Silva et al., 2012). In the Paleozoic rocks of Ardennes, two remagnetization events were recognized and the Givetian is described in detail by Zegers et al. (2003). The first event corresponds to an early Permian P-component and the second to a Carboniferous C-component. The P-component likely resides in pyrrhotite and is spatially correlated with Mississippi Valley Type (MVT) ore deposits, while the C-component is carried by SP-SD magnetite and is interpreted as formed during the smectite to illite transition. Zegers et al. (2003) recognized two main MVT districts in Belgium, the northern Namur-Verviers district and the southern Dinant district. The FF and the LT sections are not located in these districts.

The Givetian stratigraphy in the study area consists of five stratigraphic units, which are in ascending order the Hannonet (HAN), the Trois-Fontaines (TRF), the Terres d'Haurs (TRH), the Mont d'Haurs (MHR) and the Fromelennes (FRO) formations (Bultynck and Dejonghe, 2001) (**Figure 1C**). In terms of conodont biostratigraphy, the interval covered in

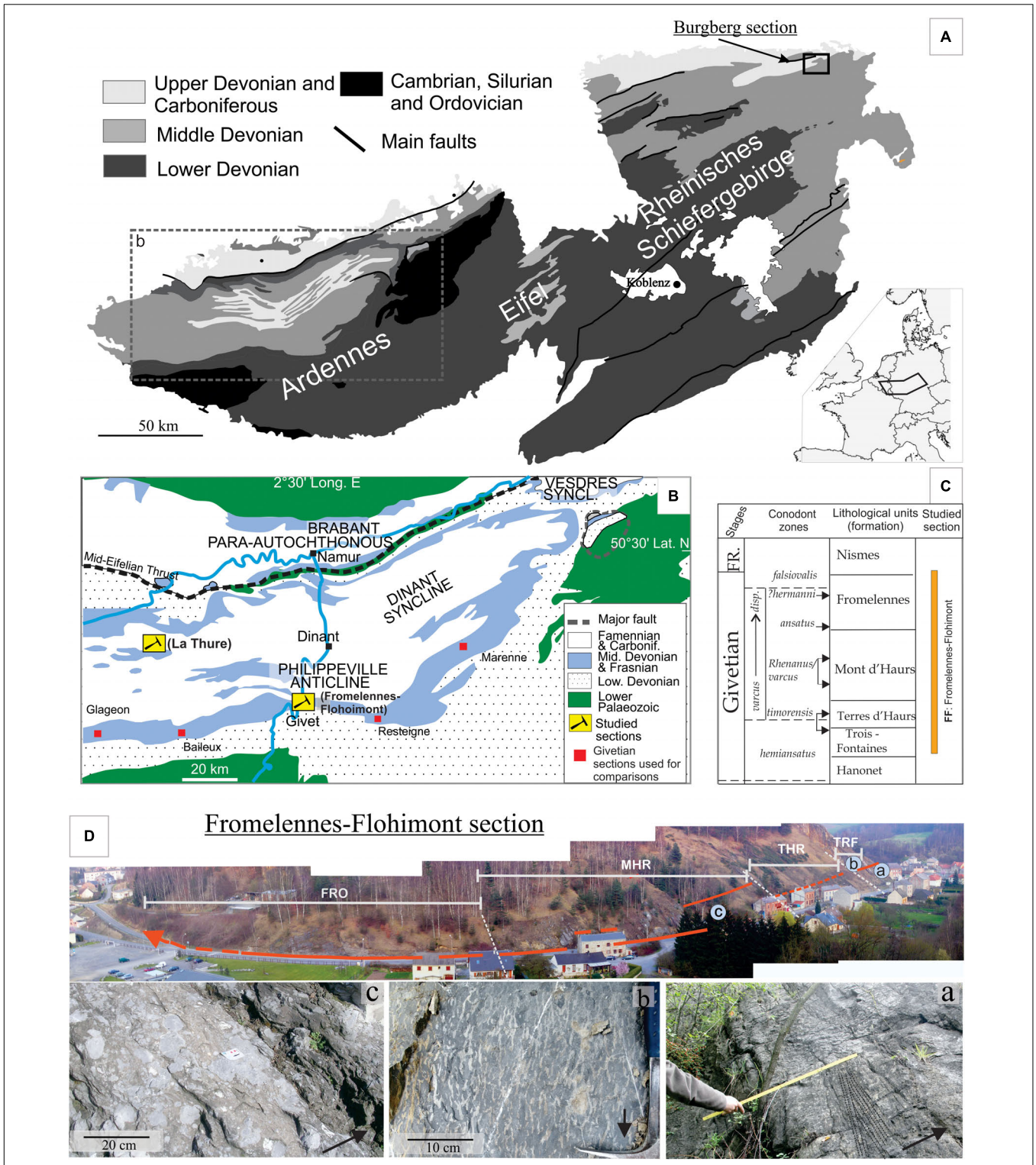

FIGURE 1 | Geological setting. **(A)** Location of the Ardennes, Eifel and Rheinisches Schiefergebirge on a simplified geological map of the Rhenohercynian Massif, modified after Wehrmann et al. (2005). For the location of this Pre-Mesozoic Massif in a present day situation see inset in the western European map in the lower right of **(A)**. The Burgberg section is situated in the upper right of **(A)**. **(B)** Simplified geological map of southern Belgium with location of the Fromelennes-Flohimont (South of the Dinant Syncline) section and La Thure (NW of the Dinant Syncline) section used for comparison in the discussion. For location of the Haine-Sambre-Meuse Overturned Thrust sheets refer to the map of Belanger et al. (2012). **(C)** Givetian lithostratigraphic column established for the southern border of the Dinant Syncline showing lower Givetian to lower Frasnian formations and conodont zones (Bultynck and Dejonghe, 2001). In Column conodont zones:

(Continued)

FIGURE 1 | Continued
timorensis Zone, the upper arrow indicates the base of the zone according to Bultynck (1987), the lower arrow, the base of the zone based on the graphic correlation method (Gouwy and Bultynck, 2003); *rhenanus/varcus* Zone, the upper arrow indicates the base of the zone according to Bultynck (1974), the lower arrow, the base of the zone based on the graphic correlation method (Gouwy and Bultynck, 2003). The interval covered by the Fromelennes-Flohimont sections is showed along the lithostratigraphic column. **(D)** Fromelennes-Flohimont road section showing the four investigated formations (white lines), the sampling track (red lines) and the exact location of pictures below. **(a)** Hummocky-cross stratification within limestone belonging to the lowest part of the Trois-Fontaines Fm. **(b)** Blue-gray limestone showing abundant cm-sized beige vertical burrows belonging to the upper part of the Trois-Fontaines Fm. **(c)** m-thick stromatoporoids-rich limestone beds characteristic of the Mont d'Haurs Fm. For an overview of the La Thure section refers to Pas et al. (2017).

the FF section extends from the lower Givetian *Polygnathus hemiansatus* Zone to the early Frasnian *Palmatolepis falsiovalis* Zone (Bultynck, 1987; Gouwy and Bultynck, 2003; Narkiewicz and Bultynck, 2010). According to Bultynck (1987), the Upper *varcus* and the *hermanni-cristatus* zones are not recognized in the FF section. Additionally, Gouwy and Bultynck (2003) indicated that the *semialternans*, *hermanni-cristatus* and *disparilis* Zones are not recognized in the Ardennes due to lack of guide species, but based on graphic correlation method the latter authors were able to locate the boundary between the *hermani* and the *disparilis* zones (see p. 326 in Gouwy and Bultynck, 2003 for detailed explanations). The portion of the LT section used for comparison herein covers a slightly shorter interval extending from the lower Givetian *Polygnathus varcus* Zone to the early Frasnian *Palmatolepis falsiovalis* Zone (Pas et al., 2015, 2017).

The Burgberg section in the northeastern portion of the Rhenohercynian Massif cut through the southeastern fore-reef fringe of the large atoll-like Brilon Reef Complex and the Hauptgrünsteinzug volcanic complex at the base. It covers a well-constrained stratigraphic interval extending from the Middle Givetian (Middle *varcus* Zone) to the Viséan (*bilineatus* Zone) which is characterized by nine depositional settings organized into off-reef, intermediate fore-reef, and proximal fore-reef main sedimentary domains (Pas et al., 2013). Major sedimentary processes occurring on this portion of the platform are gravity flows (turbidite, debris and grain flows), pelagic sedimentation (settling) and reworking of sediments triggered by storms.

METHODOLOGY

For this study we generated data on microfacies, whole rock geochemistry and hysteresis measurements in the FF section to complement the published magnetic susceptibility dataset (De Vleeschouwer et al., 2015). Hysteresis measurements were also generated for the LT section to further test the preservation of the magnetic susceptibility data reported in De Vleeschouwer et al. (2015) and Pas et al. (2017). Multi-proxy data from the FF section are then compared with new and available datasets in the LT section. The comparison of sedimentological, magnetic susceptibility, whole rock geochemistry and hysteresis measurement from the FF section with the LT datasets will allow better understanding of the origin of the magnetic susceptibility in order to interpret long distance correlations. Our analyses is based on ∼800 magnetic susceptibility samples from FF (De Vleeschouwer et al., 2015) and 31 hysteresis magnetic measurement (11 for the LT and 20 for the FF), 550 thin-sections for the FF and 41 major and trace element analyzes. To be representative of the stratigraphic successions, hysteresis and geochemical samples were taken at regular intervals all along the FF and LT sections.

Sedimentology

A detailed bed by bed description and sampling of Fromelennes-Flohimont section (461 m-thick; **Figure 1C**) was performed with a sampling interval of 25–45 cm, depending on outcrop condition. From the ∼800 samples collected across the section, 550 were used for thin-section analyses. Microfacies description was carried out following the same procedure as in Pas et al. (2017) and are described in full in **Supplementary Text 1**. Because the FF section is a lateral equivalent of the La Thure section, the microfacies described for this section should be similar to those previously described in La Thure (Pas et al., 2017). Therefore, to denote microfacies we used a similar system as in Pas et al. (2017), which relates to both the model type (DS – Drowning shelf, RS – Rimmed shelf, and RP – Ramp) and the studied locality (FF – Fromelennes-Flohimont). When microfacies described in this study were the same than those already published in Pas et al. (2017) (e.g., RS3-LT4) the label "LT" was used to avoid new layers of labeling. Finally, to build a comprehensive sedimentological model for the Givetian Ardennes platform, microfacies labels as in Pas et al. (2017) had to be adjusted. To avoid any confusion we provided an update of the LT microfacies (see table in **Supplementary Text 1**).

Rock Magnetic Analysis

Magnetic susceptibility data for this study are based on De Vleeschouwer et al. (2015). All samples collected along the FF and LT sections had their magnetic susceptibility measured, this included ∼800 samples in FF and ∼400 in the La Thure section. Magnetic susceptibility (χ) measurements (m^3/kg) were performed on a KLY-3S instrument at room temperature on samples weighing between 15 and 45°g (AGICO, noise level 2 $x10^{-8}$ SI) at the University of Liège (Belgium). Each data point is the average of three measurements. Samples were weighed with a precision of 0.01°g, which allowed the determination of the low-field mass-normalized magnetic susceptibility for each sample. χ data for Burgberg section were measured on 340 samples following a similar protocol (Pas, 2015) as the one used for the LT and FF sections.

Hysteresis loop measurements, acquisition of isothermal remanent magnetization (IRM), backfield curves and short-term remanence decay were measured with a J-coercivity rotational magnetometer developed by Kazan University (Burov et al., 1986), located at the Geophysical Centre of the Royal

Meteorological Institute of Dourbes in Belgium. Hysteresis loop measurements were carried out on 20 samples from the FF section and 11 samples from the LT section. All samples were cut into cubes (approximatively 0.9 × 0.7 × 2.5 cm) and weighed with a precision of 0.001 g. Remanent and induced magnetization were measured between +500 and −500 mT with average field increments of 0.5 mT per magnetization step. The magnetization duration at each magnetization step is in the order of tenths of a second. The high field remanence (%) is measured on the remanence backfield curve and corresponds to the difference between the measured field at 300 mT and at 500 mT (e.g., influence of high coercivity minerals). When the backfield curve is finished, the direct current is switched off automatically and the magnetizing field decreases toward a constant residual field of about 0.4 mT within the following 0.4 s. The decay of the remaining remanence (IRM 500 mT, 0.4 s) is monitored over 100 s, and is called the short-term remanence loss. The following parameters were extracted from the hysteresis loops: saturation magnetization M_s (Am^2/kg); remanent saturation magnetization, M_{rs} (Am^2/kg); high-field magnetic susceptibility (χ_{HF}, mł/kg) and coercive force H_c (mT). With the J-coercivity meter high-field susceptibility is measured only between 400 and 500 mT. The slope at high-field corresponding to the high-field magnetic susceptibility (χ_{HF}) is indicative of paramagnetic/diamagnetic contributions to the low-field magnetic susceptibility, if high coercivity minerals such as goethite and hematite are not present. When the IRM_{300}/IRM_{500} ratio is higher than 5%, the high-field slope cannot be used for slope correction and hence the values M_s, H_c, χ_{HF}, M_{rs}/M_s and H_{cr}/H_c are not regarded as reliable for interpretations. M_s, M_{rs}, and χ_{HF} were normalized with respect to sample mass. χ_{HF} thus corresponds to the high-field susceptibility values and represents a direct quantification of the combined diamagnetic/paramagnetic components for rocks that do not contain high-coercivity minerals such as hematite. The normalized decay viscosity coefficient (S_d) is calculated from the remanence decay measured during 100s. S_d represents the slope in the IRM_{500mT} versus Log_{10} (time[s]) diagram. The value χ_{ferro} (mł/kg) corresponds to the ferromagnetic *s.l.* contribution and is calculated by subtracting χ_{HF} from χ (e.g., Walden et al., 1999). Parameters extracted from the hysteresis loop are commonly interpreted using the so-called "Day" plot (Day et al., 1977) which corresponds to linear or logarithmic plot of M_{rs}/M_s and H_{cr}/H_c usually including four grain-size categories, from the coarser to the finest: multidomain (MD), pseudo-single domain (PSD), single domain (SD) and super paramagnetic (SP). Coarser grains (SD or MD) are often interpreted as detrital in origin (Parry, 1982; Königshof et al., 2016), while the smallest grains (SP and PSD) are interpreted as being formed under diagenetic conditions (Channell and McCabe, 1994).

Whole Rock Geochemistry

Major and trace element concentrations in the FF section were generated from 41 samples using X-ray Fluorescence (ARL 9400 XP XRF instrument) at the University of Liège. Precision and accuracy were both shown to be better than 1% for major elements and 5% for trace elements as controlled using 40 international and in-house standards (list available in **Supplementary Table 1**) and analyses of replicate samples, respectively.

RESULTS

Sedimentology

The measured section is ∼460 meters thick with strata oriented N65°E and a dip of 63°S (**Figure 1**). It can be divided into seven lithological units (FFU1-7, described in **Supplementary Text 1**). According to the Belgian lithostratigraphic chart defined by Préat and Bultynck (2006) and the geological map of Mansy et al. (2006), The Trois-Fontaines (TRF), the Terres d'Haurs (THR), Mont d'Haurs (MHR), and Fromelennes (FRO) formations can be identified. FFU1-2 corresponds to the Trois-Fontaines, FFU3-4 to Terre d'Haurs, FFU5 to Mont d'Haurs and FFU6-7 to the Fromelennes formations. Thickness of the above mentioned formations in the Fromelennes-Flohimont section are consistent with their thicknesses defined in the type area (see **Figure 1C**). Description of each formation and lithological units is detailed in **Supplementary Text 1**.

The field observations (e.g., facies geometry and sedimentary structures) and petrographic analyses of thin-sections (e.g., matrix, grain size, fossil content, mineralogy, etc.) allowed to the discrimination of 17 microfacies across the FF section. Specific microfacies for the Givetian in the FF area are presented in **Figure 2** and a full list of microfacies including key features and interpretations is available in **Table 1** (for an extended descriptions and interpretations of individual microfacies see **Supplementary Text 2**). Following the definition of Read (1985) for carbonate platform models, we have organized our microfacies across three main platform profiles: (1) a homoclinal ramp (RP), (2) a rimmed shelf (RS), and (3) a drowning shelf (DS). Vertical microfacies evolution in FF (**Figure 2**) indicates major changes in the depositional record, allowing reconstruction of the main sea-level fluctuations in the southern part of the Ardennes platform (**Figure 2**). These important sedimentological changes are numbered depositional intervals (I) to (VI).

Stratigraphic Evolution of the Magnetic Susceptibility Values

The Fromelennes-Flohimont χ record was first published in De Vleeschouwer et al. (2015) and for the purpose of this study we divided the curve into seven Magnetic Susceptibility Units (MSU-I to MSU-VI, **Figure 2**), based on visual evaluation of the magnetic susceptibility values. MSU-I shows average χ values of $0.08 \pm 0.1 \times 10^{-7}$ m^3/kg (see vertical dotted line in **Figure 2**). MSU-II records the highest average χ value of the entire section ($1.79 \pm 1.1 \times 10^{-7}$ m^3/kg). MSU-III also records high average values of $1 \pm 0.48 \times 10^{-7}$ m^3/kg, with important variations from 0 to 2×10^{-7} m^3/kg. The MSU-IV shows a low and monotonous signal with an average of $0.10 \pm 0.17 \times 10^{-7}$ m^3/kg. MSU-V records an average χ value of 0.48 ± 0.26 10^{-7} m^3/kg. MSU-VI exposes low χ values ($0.14 \pm 0.16 \times 10^{-7}$

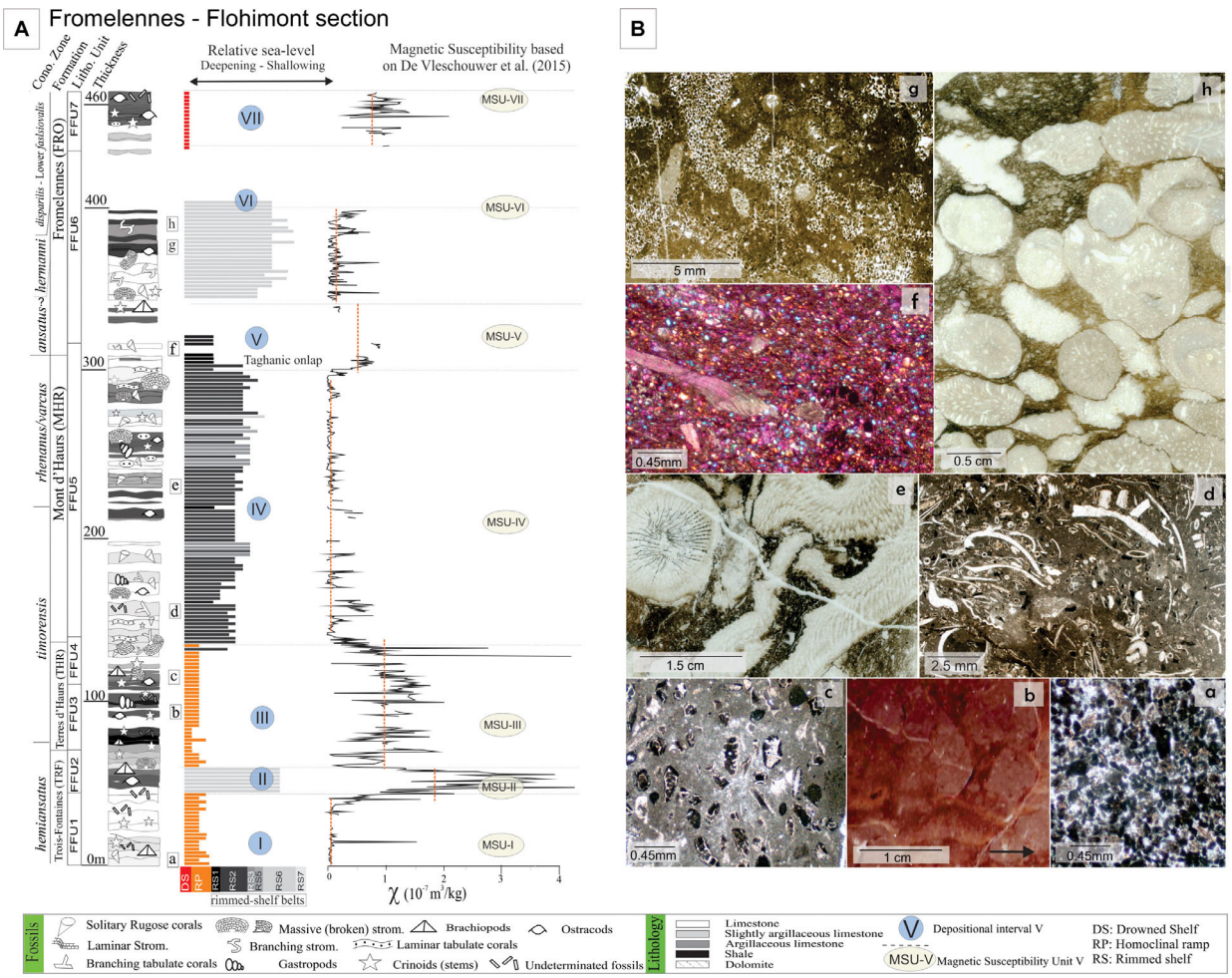

FIGURE 2 | Overview on the Fromelennes-Flohimont sequence. **(A)** Schematic sedimentological log showing formations, main lithological features, microfacies evolution with the depositional intervals (I–VI), magnetic susceptibility curve (De Vleeschouwer et al., 2015) with Magnetic Susceptibility Unit (MSU) and conodont zones (Bultynck and Dejonghe, 2001; Gouwy and Bultynck, 2003; Narkiewicz and Bultynck, 2010). Division of the magnetic susceptibility curve into seven MSU is based on visual evaluation and the symmetry with depositional intervals. **(B)** Overview of the most represented microfacies in the section **(a–h)**. **(a)** RP-FF2a: fine-grained peloidal grainstone (FRO-3, transmitted light). **(b)** PF7-FF7: red clay showing numerous occurrence of mm- to cm-sized intraclast floating in the matrix (FRO39a, transmitted light). **(c)** RP-FF1: thallus of palaeosiphonocladale filled by a darker micrite contrasting with the lighter surrounding micrite (FRO89, transmitted light). **(d)** RP-FF1: shell-rich bioclastic wackestone-packstone (FRO140, transmitted light). **(e)** RS2-LT2: reef-builders rudstone showing tabulate and rugose corals (FRO170, scanned thin-section). **(f)** RS1-FF1 off-reef shelf: brachiopods and rare crinoids in an argillaceous matrix rich in silt-sized quartz grains (FRO219, crossed nicols with gypsum blade). **(g)** PF6-FF6: densely bioturbated mudstone with bioturbations filled by a peloidal grainstone texture (FRO299a, transmitted light). **(h)** PF6-LT12: *Stachyodes* and *Amphipora* rudstone (FRO289a, scanned thin-section).

m^3/kg). MSU-VII shows a relatively high average χ value close to $0.74 \pm 0.26 \times 10^{-7}$ m^3/kg.

Magnetic Measurements and Depositional Proxies

Before χ records can be considered as a tool for stratigraphic correlation, it must be established that the χ signal still contains original paleoenvironmental information (e.g. Da Silva et al., 2013). This is not trivial in the Ardennes, where Late Variscan remagnetization events were recognized by Zegers et al. (2003). To estimate the preservation of the χ records in the FF and LT sections published in De Vleeschouwer et al. (2015), we have performed hysteresis magnetic measurements for both sections and compared the different hysteresis parameters (**Tables 2**, **3**) with the magnetic susceptibility data (e.g., Riquier et al., 2010; Da Silva et al., 2012, 2015).

The FF and LT sections show relatively similar hysteresis loops (mainly wasp-waisted shape with a positive or negative high-field slope and general high level of noise) and magnetic characteristics (**Figures 3**, **4** and **Tables 2**, **3**). After the slope correction, the ferromagnetic contribution is visible and loops appear to be wasp-waisted, and commonly show a high level noise. M_s data are well-correlated with χ for both sections (correlation coefficient $r = 0.95$ and 0.98 respectively for FF and LT). The correlation is even higher between χ_{ferro} and χ (La

TABLE 1 | Synthesis of microfacies for the Givetian in the Fromelennes-Flohimont road section (N. France).

Microfacies number	Name	Main diagnostic features	Bedding, color and sedimentary structures	Depositional setting
Drowning shelf (DS)				
DS-LT	Brachipod-bivalve shells packstone-rudstone	Limestone with brachiopods, bivalves, gastropods, crinoids. Sediment is poorly- to moderately-sorted and bioturbations are common	Decimetre thick homogeneous dark-gray to black limestone beds	Drowned lagoonal setting above the FWWB
Homoclinal ramp (RP)				
RP2-FF1	Palaeosiphonocladale and shell-rich bioclastic wackestone-packstone	Abundance of palaeosiphonocladales and crinoids. Common occurrence of brachiopods, gastropods, trilobiltes. Abundant bioclastic hash	Cm- to dm-thick fine-grained beds	Mid- to distal-ramp below the FWWB with storm deposits
RP2-FF2a	Fine-grained peloidal grainstone	Coarse-grained crinoids (with micritized rims), gastropods (with common micrite filling internal molds) and bioturbations	Cm- to dm-thick argillaceous black to dark-gray limestone beds	Mid- to distal-ramp below the FWWB with storm deposits
RP2-FF2b	Peloidal bioclastic grainstone with palaeosiphonocladales	Abundance of peloids and palaeosiphonocladaes within a grainstone texture	Cm- to dm-thick fine-grained beds	Mid-ramp within the FWWB
Rimmed shelf (RS)				
Facies belt 1: Fore-reef shelf and off-reef				
RS1-FF1	Argillaceous crinoidal – brachiopods mudstone	Crinoids, brachiopods and trilobites. Slightly argillaceous micrite rich in silt-sized quartz grains and local mica sheets	Strongly weathered argilaceous limestone	Fore-reef to off-reef setting below the FWWB
Facies belt 2: marginal reef and fore-reef shelf				
RS2-LT1	Open-marine bioclastic wackestone-packstone	Crinoids, brachiopods, ostracods, trilobites, bryozoans, tentaculitids and local debris of branching tabulate and rugose corals, and stromatoporoids	Dm thick coarse-grained dark-blue limestone beds	Open-marine setting located below the FWWB and influenced by reefal-construction (barrier-or patch-reef)
RS2-FF2	Fine- to coarse-grained crinoidal bioclastic packstone	Abundant large-sized crinoids, common brachiopods and bioturbations, ostracods, peloids, gastropods, bryozoans, rugose corals, girvanella lumps, trilobites	Dm-thick coarse-gained beds	Crinoidal meadow flanking fore-reef slope below FWWB
RS2-LT2	Coral-stromatoporoid rudstone and flaotstone	Dm-sized stromatoporoids (laminar and buldous), solitary rugose corals, branching tabulate corals, crinoids, brachiopods, trilobites	Coarse-grained dark-blue to dark-gray limestone with large and broken reef-builders in non-living position	Open-marine setting located below the FWWB in the vicinity of reef
RS2-FF3	Dendroid stromatoporoid and bioclast-rich rudstone	*Stachyodes, Amphipora* and open-marine bioclasts such as brachiopods, crinoids. Rugose and tabulate corals, peloids, grivanella and palaeosiphonocladales	Dm-thick coarse-gained beds with visible reef-builder organisms	Fore-reef open-marine setting influenced by internal shelf setting
Facies belt 3: marginal shelf sand shoals				
RS3-LT4	Peloidal – lithoclastic grainstone with gastropods and mud-coated grains	Peloids and micritic lithoclasts, gastropods, brachiopods, crinoids, ostracods and rare tabulate corals and bryozoans	Dm-thick dark blue to dark-gray limestone	Peloid shoal in the FWWB
Facies belt 5: internal restricted shelf				
RS5-LT10	Oolite lithoclastic grainstone – packstone	Type 4 ooids of Strasser (1986)	Cm- to dm-sized light- to dark-gray bed	Lagoonal setting with local higher energy-event
Facies belt 6: Internal evaporitic - brackish shelf				
RS6-LT12	Dendroid stromatoporoid flaotstone to rudstone	*Stachyodes* and *Amphipora*, *Girvanella*, *Renalcis* lumps and stromatoporoids	Pluri-dm-sized beds with local erosive base	Dendroid stromatoporoids patch-reef reworked in lagoonal setting
RS6-FF4	Micritic lithoclast and peloidal grainstone	Abudance of variously-shaped and sized peloids and lithoclasts (micritic or peloidal grainstone. Locally, *Amphipora,* ostracods, calcisphere, allocthtonous ooids	Dm-to pluri dm-sized beds	Tidal channel in the vicinity of intertidal pond and *Amphipora* patch-reefs
RS6-FF5	Mudstone-wackestone with green algae, ostracods and gastropods	*Abundance of kamaena*, *triangulinella and* ostracods. Locally gastropods, *labyrinthoconus*, *Amphipora,* peloids, calcisphere, ortonella and fenestrae	Cm- to dm-thick beds	Brackish lagoonal setting under the FWWB

(Continued)

TABLE 1 | Continued

Microfacies number	Name	Main diagnostic features	Bedding, color and sedimentary structures	Depositional setting
RS6-FF6	Mudstone	Limited flora and fauna, bioturbation filled with peloids and rare ostracods	Dm-thick beds	Evaporitic intertidal ponds
RS6-LT14	Laminated mudstone – peloidal grainstone	Alternation of peloidal grainstone and mudstone layer or light and darker micritic laminae with locally well-spread silt-sized quartz	Dm-thick beds	Tidal-channel and levees bordering channel and intertidal pounds in supratidal setting
Facies belt 7: Supratidal shelf				
RS7-FF7	Palaeosoils	Intraclast in argillaceous matrix. Intraclasts are mudstone in texture and show palaeosiphonocladale, ostracods, calciphere	Dm-thick bed showing brecciated fabric	Palaeosoils in internal supratidal shelf setting

Thure $r = 0.99$; Fromelennes-Flohimont $r = 0.99$; **Figure 4B** and **Table 3**). The nature of ferromagnetic *s.l.* fraction is investigated through the measurement of the coercive force (H_c) and the coercivity of remanence (H_{cr}). H_{cr} and H_c values in our datasets are respectively in the range of 30–70 mT and 0–15 mT and not correlated with χ values (**Figures 4C,D**). Generally, H_{cr} and H_c values are predominantly low regardless of the χ values, which is typical for carbonate platform sediments (Borradaile et al., 1993; Da Silva et al., 2012). As shown in **Figures 4C,D** few samples from the LT and FF section record H_{cr} or H_c values higher or in the range of threshold values for low-coercivity minerals like magnetite (Fe_3O_4). The IRM_{300}/IRM_{500} ratios for FF samples are predominantly lower than 5%, while half of the LT samples record ratios higher than 5%. All samples with IRM_{300}/IRM_{500} ratios higher than 5%, corresponding to non-saturating IRM curves (e.g., **Figure 3**) are shown in **Table 2** and presented along the lithostratigraphic and chemostratigraphic profiles for LT an FF sections in **Figure 5**. When low-coercivity minerals are the main contributor to the χ signal in the dataset (IRM_{300}/IRM_{500} ratios < 5) it allows the use of the high-field magnetic susceptibility (χ_{HF}) results to determine the diamagnetic/paramagnetic contributions in our samples (Sardar Abadi et al., 2015; Königshof et al., 2016). Correlation between χ and χ_{HF} is relatively good for the FF ($r = 0.64$) and the LT ($r = 0.65$) sections (**Figure 4E**) and χ_{HF} values are mostly positive in both sections.

To assess the magnetic grain size distribution in our dataset we plot ratios M_{rs}/M_s and H_{cr}/H_c for samples with IRM_{300}/IRM_{500} ratios $< 5\%$ in the bi-logarithmic "Day" diagram (Day et al., 1977; Dunlop, 2002) (**Figure 6**). Most of our data fall between or along the SD + SP (Dunlop, 2002) and MD + SD (Parry, 1982) mixing lines, which is comparable to the data of for Devonian Pelagic limestone and mudstone from Germany (Riquier et al., 2010) and the Zwing et al.'s (2005) platform carbonates in Germany. The occurrence of superparamagnetic grains, in the analyzed dataset was evaluated by the value of the decay viscosity coefficient S_d. Most samples in the dataset show high S_d values with a median of 26 and 33, respectively, for FF and LT (**Table 3**).

To evaluate the depositional origin of our χ signal we compared the stratigraphic evolution of the χ signal with the corresponding profiles for detrital proxies such as TiO_2, Al_2O_3, K_2O, Zr, and Rb (Calvert and Pedersen, 2007; Śliwiński et al., 2012; see **Table 4** for detailed geochemical datasets). As presented in **Table 3** and in **Figures 4A,B**, the correlation coefficient r between χ values and detrital input proxies for LT and FF sections shows intermediate values (r between 0.51 and 0.61 for LT section and 0.62 to 0.70 for the FF section).

To analyze how χ is facies-dependent in our sediments and even more so in the Givetian Ardennes carbonate platform, we combined published χ data (De Vleeschouwer et al., 2015) with the sedimentological models developed in this study (see section sedimentology).

Homoclinal Ramp

Sediments belonging to this profile are exposed throughout the Lower Givetian Trois-Fontaines and Terres d'Haurs formations. **Figure 5C** shows a general increase of the average χ from the mid- to outer-ramp setting, with the microfacies RP2-FF1 located at the margin between mid- and outer-ramp settings recording an exceptionally high average χ value.

Rimmed Shelf Model

The characteristic sediments in this model correspond to the middle portion of the Trois-Fontaines, the Mont d'Haurs and the Fromelennes formations. In both, the La Thure and the Fromelennes-Flohimont sections, external (RS1 and RS2) and internal shelf belts (RS3, RS4, RS5, RS6, and RS7) deposits are characterized by different χ behavior (see **Figure 5D**). A general decrease of the average χ signal from the off-reef to biostromal belts characterizes the external shelf. In the internal shelf a general increase in the average χ values is observed between the bioclastic shoals and the supratidal setting. The internal shelf oolitic shoal is marked by a decrease of the average χ values and the supratidal setting by a very high average of χ value.

DISCUSSION

Sedimentology

The sedimentological analyses of the FF section allowed the discrimination of 17 microfacies distributed over three carbonate platform types throughout the Early – Late Givetian. Major changes in the platform development can be summarized as

TABLE 2 | Magnetic susceptibility, microfacies (MF) and magnetic hysteresis parameters for each analyzed samples from FF and LT sections with the corresponding interpretations.

Samples	Position	MF	χ (10^{-8})	χ_{HF} (10^{-8})	χ_{ferro} (10^{-8})	M_s (10^{-4})	M_{rs} (10^{-4})	IRM_{300}/IRM_{500}	Mrs/Ms	H_c	H_{cr}	Hcr/Hc	S_d	Interpretation			
	m		m^3/kg	m^3/kg	m^3/kg	Am^2/kg	Am^2/kg	[%]	N/A	mT	mT	N/A	N/A	Dominating non ferro Type	Maghaemite/ Magnetite Presence	Haematite Presence	SP grains Presence
Fromelennes-Flohimont (FF)																	
FRO-10	0.3	RP2-FF2a	0.08	−0.20	0.28	1.00	0.090	4.2	0.09	12.6	50.1	3.98	25.34	Carbonate	−	−	++
FRO22A	**30.5**	**RP2-FF2a**	**0.21**	**−0.07**	**0.28**	**1.78**	**0.050**	**13.0**	**0.03**	**3.9**	**58.3**	**14.95**	**16.68**	**Carbonate**	**−**	**−**	**+**
FRO54	52.2	RS6-FF5	31.38	0.67	30.71	59.56	12.030	2.0	0.20	8.0	49.6	6.20	33.07	Clay	+++	−	++
FRO76A	72.5	RS1-FF1	10.23	0.32	9.91	16.11	3.430	2.5	0.21	8.5	47.8	5.62	26.81	Clay	++	−	++
FRO92A	90.3	RS1-FF1	13.18	0.69	12.50	24.54	5.430	2.5	0.22	9.7	49.1	5.06	27.07	Clay	++	−	++
FRO128	110.1	RS1-FF1	13.49	1.70	11.79	18.84	4.540	3.5	0.24	10.5	53.8	5.12	25.51	Clay	++	−	++
FRO151A	129.8	RS1-FF1	7.51	0.56	6.94	11.35	2.045	3.3	0.18	6.2	45.3	7.31	30.91	Clay	++	−	++
FRO173A	149.1	RS2-LT2	0.87	0.18	0.69	8.18	0.755	4.0	0.09	11.4	37.3	3.27	15.53	Clay/carbonate	+	−	+
FRO195A	**193.6**	**RS2-LT2**	**−0.33**	**−0.35**	**0.02**	**0.56**	**0.039**	**4.4**	**0.07**	**81.2**	**31.8**	**0.39**	**12.84**	**Carbonate**	**No**	**No**	**+**
FRO207C	231.3	RS2-LT2	0.99	−0.28	1.27	2.62	0.219	3.1	0.08	4.2	38.8	9.24	32.00	Carbonate	−	−	++
FRO222A	**245.0**	**RS1-FF1**	**0.94**	**−0.06**	**1.00**	**2.90**	**0.570**	**10.9**	**0.20**	**11.6**	**56.3**	**4.85**	**42.62**	**Carbonate**	**−**	**+**	**+++**
FRO246A	269.8	RS5-LT10	0.39	−0.10	0.49	2.64	0.320	4.4	0.12	7.8	45.4	5.82	19.45	Carbonate	+	−	+
FRO263A	289.9	RS5-LT10	0.24	−0.19	0.43	0.73	0.120	0.5	0.17	8.0	49.4	6.18	19.06	Carbonate	+	−	+
FRO272B	300.0	RS2-LT1	5.51	0.28	5.23	13.22	1.850	2.0	0.14	5.1	42.7	8.37	33.66	Clay	++	−	++
FRO280B	**313.0**	**RS2-LT1**	**8.15**	**0.91**	**7.24**	**9.29**	**1.690**	**5.4**	**0.18**	**7.6**	**48.5**	**6.38**	**28.86**	**Clay**	**++**	**+**	**++**
FRO292B	351.5	RS6-LT12	0.06	0.77	−0.72	14.86	2.310	2.4	0.16	6.5	44.8	6.89	26.72	Clay	++	−	++
FRO317	370.2	RS6-LT12	1.43	−0.24	1.67	1.92	0.212	3.0	0.11	15.4	46.7	3.03	12.14	Carbonate	+	−	−
FRO354B	394.1	DS-LT	1.46	−0.16	1.61	3.60	0.254	1.4	0.07	3.3	34.9	10.58	35.46	Carbonate	+	−	++
FRO362A	440.7	DS-LT	7.37	0.23	7.14	12.49	2.477	3.1	0.20	6.9	44.7	6.48	28.84	Clay	++	−	++
FRO400	461.2	DS-LT	6.60	0.19	6.41	7.76	1.297	2.2	0.17	6.4	43.1	6.69	30.32	Clay	++	−	++
La Thure																	
TUR100	0.1	RS2-LT1	6.37	−0.10	6.47	16.16	1.28	4.0	0.08	3.7	47.9	12.95	40.60	Carbonate	++	+	+++
TUR121	**10.2**	**RS4-LT8**	**2.87**	**0.00**	**2.86**	**4.62**	**1.06**	**5.4**	**0.23**	**7.0**	**49.8**	**7.11**	**33.78**	**Carbonate + clay**	**++**	**+**	**++**
TUR158	**34.9**	**RS5-LT15**	**7.58**	**0.03**	**7.55**	**14.35**	**2.13**	**6.5**	**0.15**	**4.2**	**46.0**	**11.06**	**63.06**	**Carbonate + clay**	**+**	**+**	**+++**
TUR163d	**39.6**	**RS3-LT4**	**2.52**	**0.00**	**2.52**	**4.93**	**0.84**	**5.6**	**0.17**	**7.4**	**51.7**	**7.00**	**32.06**	**Carbonate**	**+**	**+**	**++**
TUR181b	53.8	RS5-LT10b	1.62	0.00	1.62	1.97	0.24	4.2	0.12	5.2	40.9	7.90	29.69	Carbonate	+	+	++
TUR205c	69.1	RS2-LT2	3.10	−0.19	3.30	1.64	0.40	4.6	0.24	8.1	50.0	6.20	26.25	Carbonate	+	+	++
TUR233a	99.8	RS5-LT15	5.20	0.34	4.87	9.46	2.05	3.4	0.22	9.5	48.7	5.13	23.32	Clay	++	+	++
TUR241c	**105.4**	**RS5-LT15**	**1.66**	**0.16**	**1.49**	**0.94**	**0.17**	**12.9**	**0.18**	**11.8**	**60.3**	**5.09**	**22.44**	**Clay**	**−**	**++**	**++**
TUR250b	110.4	RS5-LT15	2.74	0.45	2.30	4.36	0.50	4.1	0.11	4.4	52.4	11.94	29.23	Clay	+	+	++
TUR300b	**145.6**	**RS5-LT15**	**17.09**	**0.68**	**16.42**	**46.00**	**4.85**	**10.4**	**0.11**	**5.0**	**69.8**	**13.95**	**39.74**	**Clay**	**++**	**++**	**++**
TUR306	**149.8**	**RS5-LT15**	**10.24**	**0.18**	**10.06**	**20.00**	**1.69**	**10.4**	**0.08**	**3.0**	**64.7**	**21.56**	**47.07**	**clay**	**+**	**+++**	**+++**

Bold highlights samples that have to be regarded with caution as they record IRM_{300}/IRM_{500} ratio > 5 indicating that a slope correction cannot be calculated. For a definition of each parameter, refer to the main text.

TABLE 3 | Mean value (mean) for each hysteresis parameter showing IRM_{300}/IRM_{500} ratio < 5 and correlation coefficient (*r*) between each hysteresis parameter and the magnetic susceptibility (χ).

		Hysteresis								Geochemistry				
	Number of sample (n)	χ_{HF} ($10^8 m^3/kg$)	χ_{ferro} ($10^8 m^3/kg$)	M_s ($10^4 Am^2/kg$)	M_{rs} ($10^4 Am^2/kg$)	H_c (mT)	H_{cr} (mT)	S_d	Number of sample (n)	SiO_2 % wt.	Al_2O_3 % wt.	TiO_2 % wt.	K_2O % wt.	Zr ppm
LT	**5**								**30**					
r (χ)		0.05	0.99	0.94	0.82	0.05	0.30	0.43		0.51	0.61	0.58	0.48	NM
Mean		0.10	3.71	6.72	0.89	6.17	47.99	29.82		5.00	2.00	0.10	1.01	NM
FF	**16**								**42**					
r (χ)		0.57	1.00	0.95	0.96	0.01	0.45	0.38		0.66	0.70	0.69	0.62	0.64
Mean		0.28	6.22	12.46	2.34	8.16	45.20	26.70		5.49	1.42	0.11	0.18	15.73

Right part of the table shows mean value for each detrital proxy parameters and also correlation coefficient (r) between detrital proxy parameters and χ. Magnetic susceptibility data are from De Vleeschouwer et al. (2015). NM, not measured. For a definition of each parameter, refer to the main text.

follows: (1) development of a homoclinal ramp during the early Givetian, (2) evolving to a rimmed shelf throughout the middle- to late-Givetian and (3) then by the latest Givetian the carbonate factory dramatically collapses and the platform drowns, (4) and was subsequently capped by Frasnian shales. Carbonate platform types observed in this section are similar to those described in the time equivalent LT section in NW part of the Ardennes (Pas et al., 2017). To build a reliable correlation framework between the South and the NW part of the Ardennes platform we compared microfacies defined in the FF section with those published for the in LT section and this allowed the construction of integrated sedimentological models for the ramp (**Figure 7A**) and the rimmed shelf (**Figure 7B**). The integration of both sets of microfacies also enables an insight into the vast array of depositional environments that characterize the Givetian of the Ardennes as well as their proximal – distal distribution. Due to the complexity and diversity of depositional settings defining the rimmed shelf profile, we have divided this model into seven facies belts (RS1-RS7): (RS1) fore-reef to off-reef shelf; (RS2) biostromal and fore-reef shelf; (RS3) bioclastic shoals; (RS4) internal shelf with moderate circulation; (RS5) internal restricted shelf; (RS6) internal evaporitic shelf and (RS7) supratidal shelf setting. Facies belts RS1 and RS7 do not occur in the time-equivalent LT section (Pas et al., 2017) while the facies belt RS4 is not observed in the FF section. The ramp model (RP) shows a homoclinal profile and can be divided into outer- (RP1) and mid-ramp (RP2) settings. This two belts are similarly exposed in the LT section. The drowning shelf model (DS) is also observed in the LT section and characterized by a similar facies.

Origin and Nature of the Ferromagnetic Minerals and Magnetic Susceptibility

Based on the analyses of the hysteresis loops and the comparison of hysteresis parameters with the χ signal (**Figures 3**, **4**) we provide an insight into the origin of the χ signal and the nature of the ferromagnetic susceptibility.

M_s (magnetization at saturation) and χ_{ferro} (ferromagnetic susceptibility) are both proxies for the concentration of ferromagnetic minerals. The very good correlation of χ with M_s and χ_{ferro} indicates that χ values in LT and FF sections is influenced by the ferromagnetic *s.l.* contribution. As noted in Section "Magnetic Measurements and Depositional Proxies," most of our data shows H_{cr} and H_c values that correspond to the domain of remanence coercivity values of low-coercivity minerals like magnetite/maghaemite indicating that these ferromagnetic minerals are the main contributors to the χ signal variation. This observation concurs with results established for sediments found in remagnetized carbonate platforms (Borradaile et al., 1993; Zwing et al., 2005; Riquier et al., 2010; Da Silva et al., 2012, 2013). The LT and FF samples that record H_{cr} and H_c values in the range or higher than threshold values for low-coercivity minerals like magnetite, and a IRM_{300}/IRM_{500} ratios higher than 5% are interpreted as containing a relatively high abundance of hematite grains (e.g., FRO222A, **Figure 3C**). An IRM_{300}/IRM_{500} ratios < 5 is a good indicator of non-saturating IRM curve (e.g., TUR300b, **Figure 3A**) that are characteristic for low-coercivity minerals. The absence of a negative correlation between H_{cr} or H_c and χ indicates that the hematite contribution to the bulk magnetic susceptibility is weak. This can be explained by the fact that the hematite has a remanent saturation much lower than the magnetite/maghaemite, e.g., 2.5 kA/m versus 480 or 380 kA/m.

Correlation between χ and χ_{HF} are relatively good for the FF (r = 0.64) and the LT (r = 0.65) sections (**Figure 4E**), pointing to a paramagnetic/diamagnetic mineral influence to the χ signal. FF and LT sections show both positive and negative χ_{HF} values, which indicate that high-field magnetic susceptibility contribution are either dominated by paramagnetic minerals such as clay and pyrite (positive χ_{HF} values) or diamagnetic minerals such as calcite (negative χ_{HF} values). A summary of our interpretations based on the comparison of χ with hysteresis parameters and on the analysis of hysteresis loops is provided in **Table 2**.

To estimate the main grain-size of ferromagnetic sensu stricto particles in our dataset and to assess whether or not the ferromagnetic signal was overprinted by diagenetic processes we plot ratios M_{rs}/M_s and H_{cr}/H_c obtained for the LT and FF sections in the bi-logarithmic Day diagram (Day et al., 1977) and compare it with previously published data (e.g., Jackson, 1990; Zwing et al., 2005; Devleeschouwer et al., 2010;

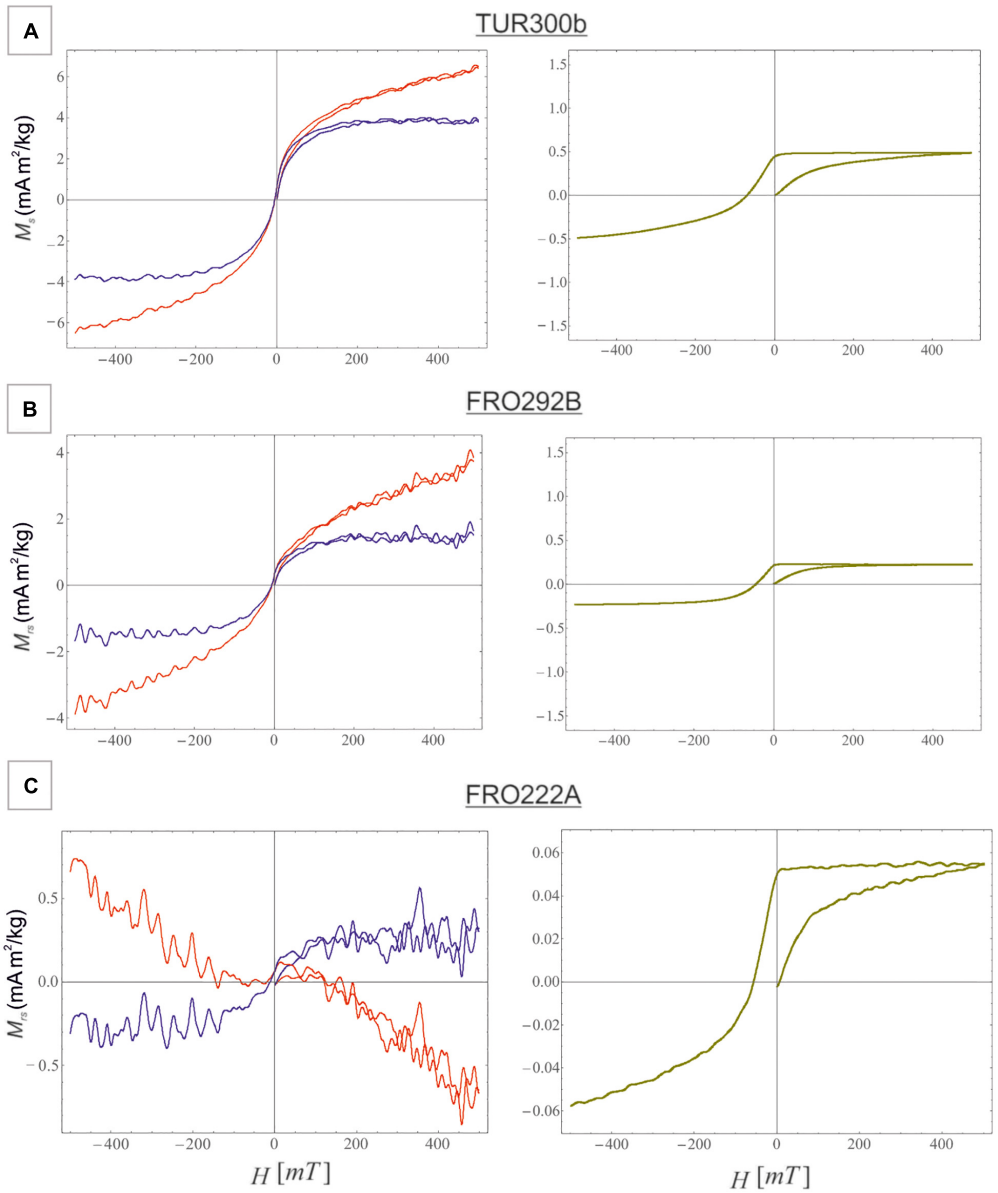

FIGURE 3 | Example of hysteresis curves and corresponding IRM acquisition curves in LT **(A)** and FF **(B,C)** sections. Right column: plots before (red) and after slope correction (blue). Left column: backfield curves.

Riquier et al., 2010; Königshof et al., 2016) and empirical trend lines for different grain-size categories (Parry, 1982; Dunlop, 2002). In this study χ versus T measurements have not been performed which hampers the ability to determine whether a mixture of different ferromagnetic minerals occurs in our dataset. In order to use the Day diagram we have made the assumption that there is no mixture of ferromagnetic minerals in the analyzed data. Indeed, interpretation of the Day diagram is ambiguous for particle size diagnosis and mineralogy when the analyzed data includes different magnetic mineralogy (Tauxe et al., 2002; Roberts et al., 2018). In their paper, Roberts et al. (2018) also discussed several other factors such the stress state, the surface oxidation, the magnetostatic interactions and particle shape that can undermine the use of the Day diagram as a tool for diagnosing domain state, particle size, or mineralogy.

The "Day" diagram in **Figure 6** reveals that our limestone samples are mostly distributed between the SD + SP mixing curve of Dunlop (2002) and the mixing SD + MD curve (Parry, 1982), similar to North America Paleozoic limestones (Jackson, 1990), Paleozoic clastic and carbonate rocks (Zwing et al., 2005) and Frasnian/Famennian limestone/shale (Riquier et al., 2010). Values from Jackson (1990) illustrated in the Day plot were interpreted by Channell and McCabe (1994) as recording a fine-grained fingerprint typical of remagnetized limestone. Data

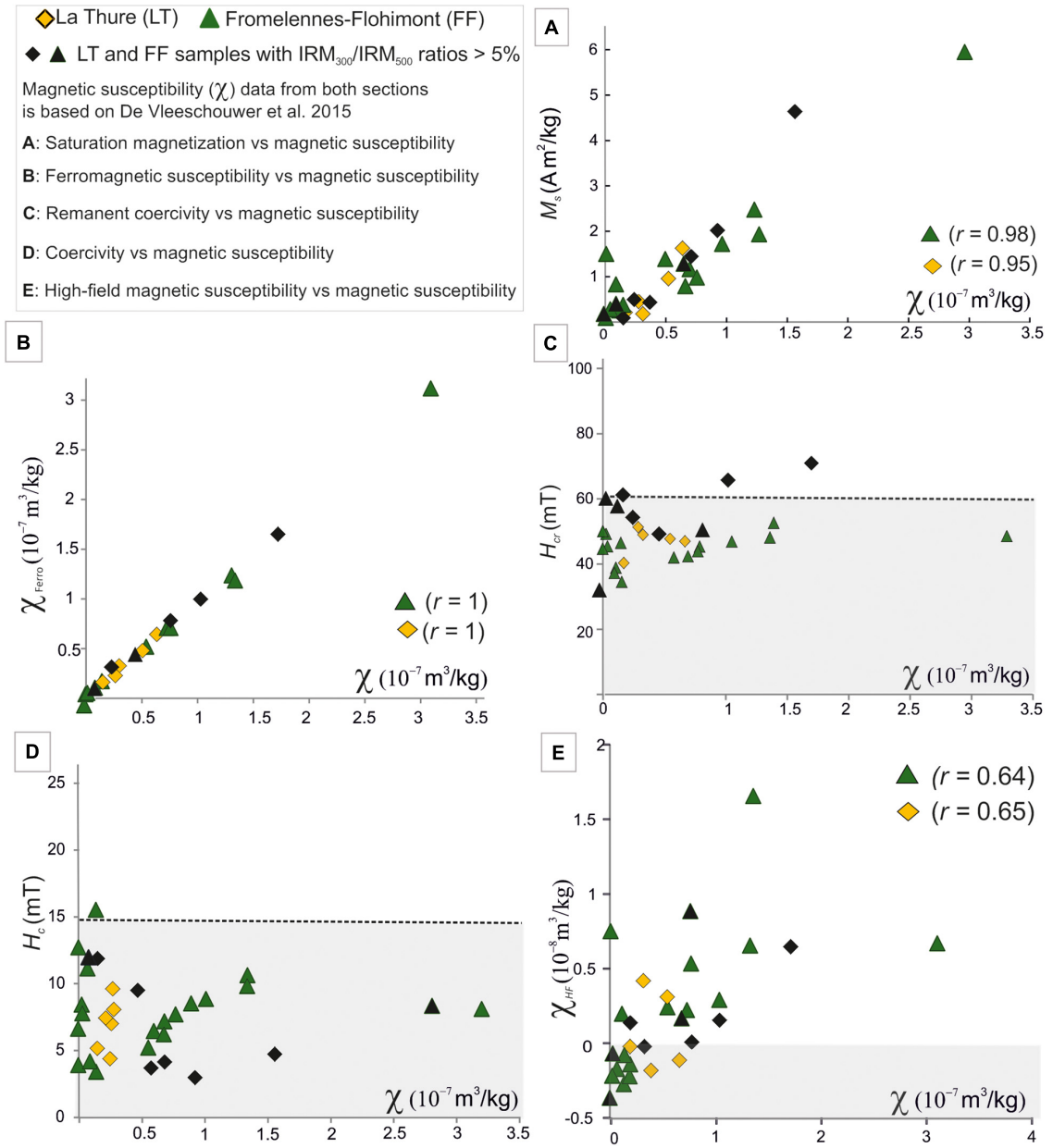

FIGURE 4 | Comparison of initial magnetic susceptibility (χ) published in De Vleeschouwer et al. (2015) with parameters extracted from the hysteresis loops for the Fromelennes-Flohimont and the La Thure sections. **(A)** Magnetization at saturation (M_s, Am^2/kg) versus χ. **(B)** Ferromagnetic susceptibility (χ_{ferro}, m^3/kg) versus χ. **(C)** Comparison of χ with the remanent coercivity (H_{cr}). The shaded band corresponds to the domain of remanence coercivity values of magnetite. **(D)** Comparison of χ with the coercivity (H_c). The Shaded band corresponds to the domain of coercivity values for magnetite. **(E)** High-field magnetic susceptibility (χ_{HF}, m^3/kg) versus χ. Shaded band corresponds to χ_{HF} negative values.

from Riquier et al. (2010) from Devonian sections in the NE Rhenohercynian Massif (Steinbruch Schmidt and Beringhauser Tunnel sections) also show a remagnetized fingerprint. Riquier et al. (2010) interpreted the magnetic signature of their samples as the superposition of a coarse-grained magnetite detrital fraction and a diagenetic fraction showing authigenic SD + SP fine-grained magnetite. Da Silva et al. (2013) studied the Devonian section in Belgium (Tailfer, Villers-le-Gambon, Moulin Bayot, Baileux) and also show a remagnetized fingerprint occurring during the Variscan Orogeny to be a consequence of the Zegers et al.'s (2003) Carboniferous remagnetization event. As described in the geological setting, the FF and LT sections are both located out of the MVT districts, which is related to the P-component of Zegers et al.'s (2003) remagnetization events. The P-component is therefore not considered as affecting the χ signal. The LT and FF samples falling close to data from Zwing et al. (2005)

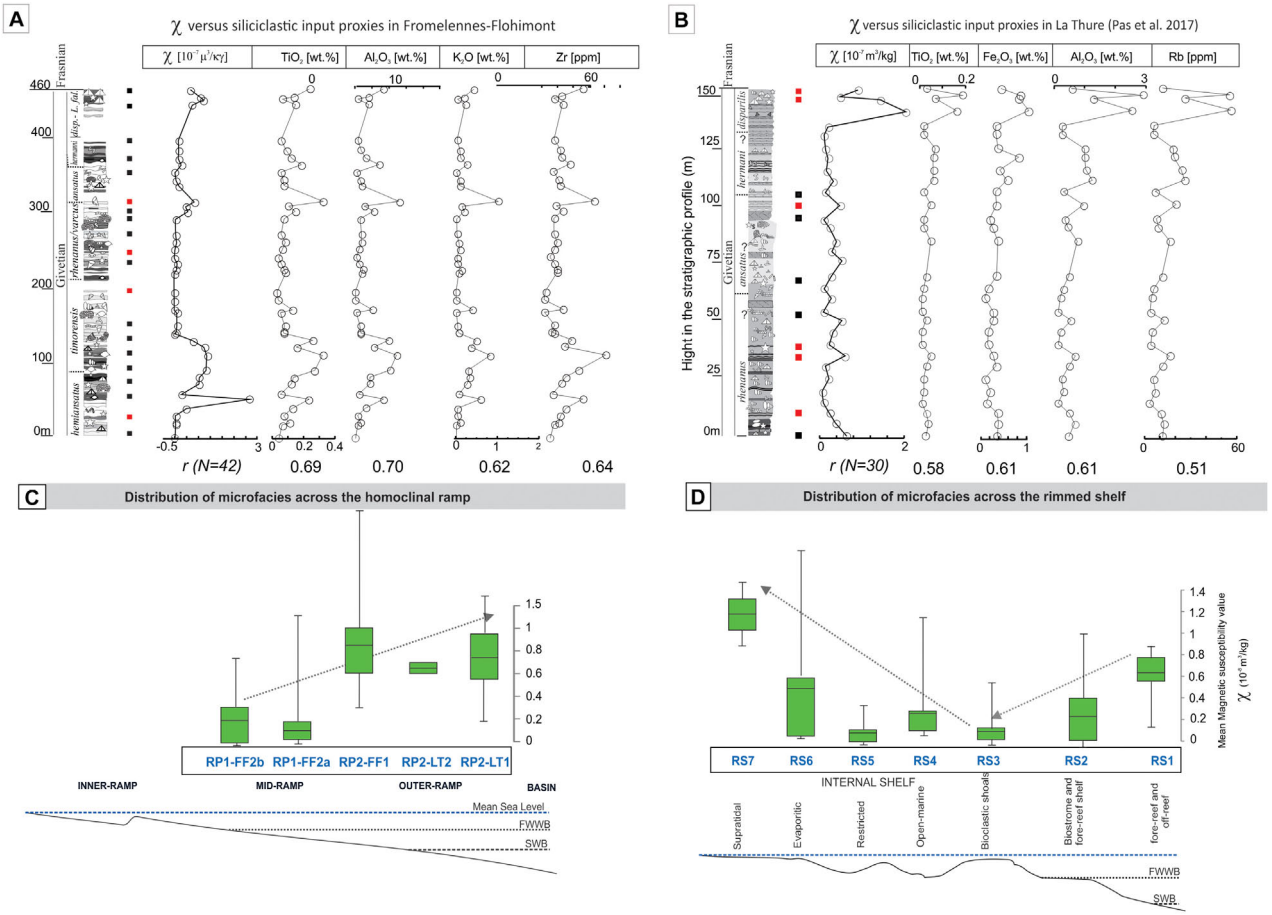

FIGURE 5 | Magnetic susceptibility versus chemostratigraphic profiles and versus sedimentological profiles. Squares along both profiles indicate the position of the samples for magnetic analyses and whether the samples record IRM_{300}/IRM_{500} ratio > 5 (red square). **(A)** Chemostratigraphic profiles of χ, TiO_2, Al_2O_3, K_2O and Zr in the FF section. Concentration of these elements are considered as proxy for detrital inputs and show moderate correlation with χ variations. **(B)** Chemostratigraphic profiles of χ, TiO_2, FeO_2, Al_2O_3, and Rb in the LT section (Pas et al., 2017) for comparison. Concentration of presented elements as proxy for detrital inputs show moderate correlation with χ variations in the LT section. Difference in the selected detrital input proxies between the studied FF section and the published LT section relates to the analytical capability differences between the XRF (used in this study of the FF) and ICP-MS (used in Pas et al., 2017 for the LT section) used for whole rock geochemistry. **(C)** Box-whisker showing median (horizontal line), range of mean 50 percent of results (shaded boxes) and extreme χ values (caps) on relative proximity transect illustrated by the position ramp-related microfacies from proximal to distal location. **(D)** Box-whisker showing median (horizontal line), range of mean 50 percent of results (shaded boxes) and extreme χ values (caps) on relative proximity transect illustrated by the position of the main facies belts (RS1-RS7) defined for the rimmed shelf model.

and Riquier et al. (2010) (**Figure 6**) are therefore interpreted as carrying a secondary signal related to the Late Variscan Carboniferous remagnetization documented by Zegers et al. (2003). For the FF samples falling near to the MD + SD mixing line of Parry (1982), a primary detrital origin could be assumed. However, as a remagnetization overprint is suggested in most of the FF samples (as discussed above), we assume that in these samples the remagnetization fingerprint is masked by the occurrence of coarser-grained (MD) detrital magnetite. Such a hypothesis was also proposed by Zwing et al. (2005) who studied various lithologies from the NE Rhenohercynian Massif extending from siliciclastic rocks to biohermal and platform carbonate.

The sections under investigation were not studied paleomagnetically and in the exception of what is indicated above, we have no direct evidence to prove the Late Carboniferous – Permian remagnetization components outlined in Zegers et al. (2003). However, the Givetian limestones in this study were collected near Givetian samples studied in Zegers et al. (2003), which are characterized by a remagnetized signature as the C-component described above. This outcome strongly supports our interpretation for the origin of the secondary magnetic grains related to the C-component.

The normalized decay viscosity coefficient S_d is another parameter that allows for estimation of fine-grained superparamagnetic (SP) and viscous grain concentration in samples. The relatively high values for the studied samples (**Tables 2**, **3**) is comparable to the S_d coefficient of SP grains contained in Tiva Canyon tuff reference samples TCO4-11M (Sd = 25 × 10-3, containing SP and SSD; Spassov and Valet,

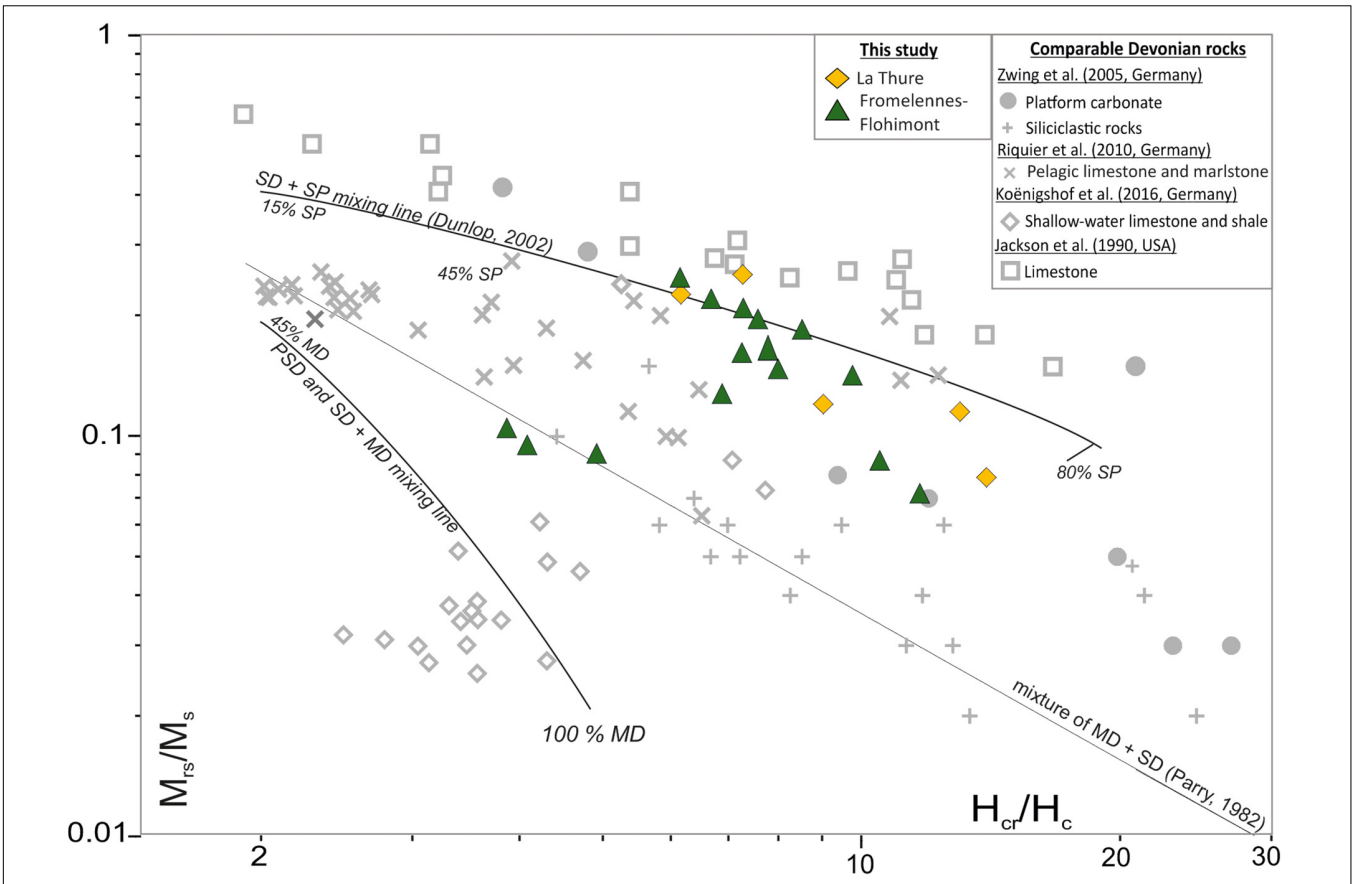

FIGURE 6 | Bi-logarithmic Day plot (Day et al., 1977) for FF and LT datasets compared with reported Paleozoic data for remagnetized siliciclastic and carbonate rocks from Jackson (1990) and Zwing et al. (2005), data from Riquier et al. (2010) and limestone/shale from Königshof et al. (2016). The lines are theoretical SD + SP and PSD and SD + MD curves from Dunlop (2002) that are based on 10 nm SP magnetite grains and coarse-grained magnetite end members, respectively. The dashed line corresponds to a mixture of MD+SD grains according to Parry (1982).

2012). This confirms the occurrence of high viscosity grains such as SP magnetic and hematite minerals in both sections, which is another argument supporting a remagnetization.

Results from Day plot (**Figure 6**), along with normalized magnetic viscosity coefficients point out that the χ signal in the LT and FF sections is triggered by the combined effect of a remagnetization and a primary detrital signature.

Magnetic Susceptibility Versus Detrital and Depositional Proxies

The delivery of detrital materials basinward is considered as the main primary-controlling factor of the χ signal (Vanderaveroet et al., 1999; Ellwood et al., 2000; Tribovillard et al., 2006; Śliwinski et al., 2010; Śliwiński et al., 2012). The ferromagnetic and paramagnetic minerals that have the strongest influence on the χ signal are predominantly derived from continental sources (Crick et al., 1997; Ellwood et al., 2001). Therefore, to interpret the primary character of a χ signal it is worth comparing χ with proxies for detrital input such as TiO_2, Al_2O_3, K_2O, Zr and Rb (Calvert and Pedersen, 2007; Śliwiński et al., 2012) (**Table 4**). To interpret the primary character of the χ signal in the FF section published in De Vleeschouwer et al. (2015), we plot the stratigraphic evolution of the χ signal against the chemostratigraphic profiles of proxy for detrital inputs (**Figure 5A**). This comparison shows similar evolution of both profiles show intermediate *r* value (*r* between 0.62 and 0.70, see also **Table 3**), indicating that the influence of detrital proxies on the χ signal is relatively strong. Pas et al. (2017) showed similar results for the LT section, when comparing the χ profile against detrital input profiles (see Figure 12 in Pas et al., 2017; *r* between 0.51 and 0.61). The relatively good correlation between the χ signal and the chemostratigraphic profiles for both the LT and FF sections indicates that the primary detrital signal is reasonably well preserved in these sections, implying that the primary χ trends could have been retained despite diagenetic or very low grade metamorphic imprints related to burial and remagnetization.

How χ values vary as a function of facies is another technique that provides an insight into the influence of syn-sedimentary parameters (e.g., Mabille et al., 2008b; Da Silva et al., 2009). Da Silva et al. (2013) analyzed a large number of Mid-Upper Belgian Devonian sections and settings (e.g., carbonate ramp, shelf and mud mounds models), and outlined a significant

TABLE 4 | Selected Major and trace element abundances for the Fromelennes-Flohimont section determined by XRF and corresponding χ value from De Vleeschouwer et al. (2015).

Samples	Position	χ	Major elements						Trace elements				
			Al_2O_3	CaO	Fe_2O_3	K_2O	SiO_2	TiO_2	Rb	Sr	Th	U	Zr
	(m)	mł/kg	wt. %	wt. %	wt. %	wt. %	wt. %	wt. %	ppm	ppm	ppm	ppm	ppm
FRO -10	0.32	8.047*E*-10	0.156	96.590	0.309	0.020	1.202	0.044	4.247	321.311	1.683	2.182	5.507
FRO 15	18.23	3.879*E*-09	0.411	98.610	0.648	0.025	0.849	0.062	4.052	277.290	2.502	−0.213	7.736
FRO 18A	20.70	3.395*E*-09	0.749	95.641	0.605	0.112	3.345	0.111	7.079	190.248	2.586	1.921	10.847
FRO 22A	30.51	2.059*E*-09	0.413	97.418	0.685	0.044	1.652	0.073	4.880	205.547	1.616	2.397	12.250
FRO 35B	39.99	4.892*E*-08	1.294	94.763	1.205	0.044	2.697	0.127	9.355	227.890	−0.208	−1.177	15.729
FRO 54	52.19	3.138*E*-07	3.420	78.185	1.218	0.591	12.614	0.235	19.691	236.104	2.840	−0.143	26.279
FRO 61A	58.60	2.673*E*-08	0.522	92.569	0.455	0.078	4.780	0.052	5.640	275.010	4.604	0.747	6.918
FRO 76A	72.52	1.023*E*-07	1.853	88.374	1.008	0.276	6.575	0.123	12.385	247.555	1.626	−1.647	12.722
FRO 88A	80.98	1.035*E*-07	1.822	85.955	1.137	0.338	8.808	0.135	12.761	313.270	2.941	1.172	15.272
FRO 92A	90.27	1.318*E*-07	4.183	77.856	1.528	0.296	13.618	0.272	27.419	326.823	6.865	0.803	23.722
FRO 128	110.10	1.349*E*-07	4.935	69.800	2.367	0.832	16.960	0.320	33.281	287.229	2.424	3.947	40.920
FRO 144	121.01	1.229*E*-07	2.361	84.470	1.781	0.362	8.640	0.152	15.960	405.477	−1.069	1.447	14.495
FRO 151A	129.79	7.506*E*-08	4.026	77.921	1.750	0.492	13.691	0.259	26.415	594.493	1.089	−0.674	19.479
FRO 161A	139.12	−1.354*E*-09	0.795	92.739	0.797	0.088	2.112	0.075	5.616	296.962	−0.480	2.184	7.778
FRO 163B	140.70	5.968*E*-09	0.741	88.026	0.506	0.063	3.107	0.071	6.391	442.167	2.187	0.229	6.031
FRO 173A	149.14	8.678*E*-09	0.665	95.175	0.428	0.047	2.961	0.080	6.050	357.228	−1.826	−1.098	8.482
FRO 180A	166.22	8.238*E*-09	0.242	95.918	0.219	0.020	2.129	0.053	3.457	586.889	−1.290	0.787	1.934
FRO 183B	169.99	−2.271*E*-09	2.094	58.758	1.212	0.417	8.380	0.128	14.724	135.783	4.961	1.176	14.012
FRO 192A	182.86	−2.533*E*-09	0.153	97.768	0.077	0.016	0.867	0.039	2.980	538.076	1.260	1.726	1.665
FRO 195A	193.63	−3.304*E*-09	0.124	97.546	0.041	0.008	0.736	0.032	3.053	440.569	4.538	−0.305	2.339
FRO 199	218.72	−3.304*E*-09	0.901	93.920	0.449	0.075	2.939	0.086	8.129	360.505	5.242	1.653	9.906
FRO 200	222.64	6.912*E*-09	1.004	80.903	0.591	0.139	2.808	0.077	6.721	223.632	1.965	−0.080	10.154
FRO 207C	231.28	9.875*E*-09	0.556	95.542	0.150	0.058	2.748	0.058	4.732	286.864	3.391	−0.154	8.159
FRO 217A	238.91	−2.329*E*-09	0.249	92.947	0.094	0.030	1.385	0.041	3.397	335.239	1.462	1.427	5.362
FRO 222A	245.03	9.352*E*-09	17.755	4.942	7.557	3.648	60.142	0.917	131.980	113.025	12.543	3.266	156.945
FRO 225A	249.79	3.157*E*-10	0.549	90.626	0.320	0.093	3.444	0.065	5.652	226.955	3.694	1.228	8.178
FRO 233A	258.90	7.556*E*-09	0.850	92.770	0.328	0.081	3.705	0.084	6.855	296.343	0.816	3.403	9.996
FRO 246A	269.84	3.863*E*-09	0.854	93.249	0.346	0.031	1.417	0.056	4.684	226.204	−0.167	4.035	7.949
FRO 263A	289.94	2.400*E*-09	0.683	87.552	0.432	0.026	0.985	0.075	5.708	386.930	−0.110	−1.098	7.889
FRO 272B	300.00	5.513*E*-08	2.272	87.271	1.012	0.209	6.941	0.146	13.167	302.134	−0.989	−1.313	13.292
FRO 278C	306.51	4.566*E*-08	1.141	84.937	1.721	0.156	8.757	0.103	7.501	425.737	1.517	3.656	9.520
FRO 280B	312.96	8.152*E*-08	5.214	70.207	2.350	1.030	17.887	0.325	29.347	290.041	4.220	0.513	33.499
FRO 282A	333.89	1.730*E*-08	0.883	56.997	1.030	0.097	6.951	0.076	6.876	123.321	2.686	1.145	12.156
FRO 285A	340.80	5.714*E*-09	0.691	70.755	0.938	0.093	3.356	0.070	6.269	154.306	0.639	−1.002	10.867
FRO 292B	351.51	5.680*E*-10	0.313	93.915	0.211	0.025	3.446	0.056	3.864	333.897	−0.984	−2.120	7.720
FRO 304C	361.44	2.693*E*-08	2.882	76.223	0.897	0.276	9.312	0.186	18.817	210.223	2.726	1.136	17.941
FRO 317	370.24	1.432*E*-08	1.286	92.927	0.619	0.125	4.447	0.123	9.338	303.078	2.802	1.597	12.493
FRO 353	380.48	1.610*E*-08	0.802	94.710	0.253	0.103	3.760	0.088	5.901	241.936	−2.320	−0.833	12.167
FRO 354B	394.12	1.458*E*-08	0.431	96.621	0.375	0.037	2.152	0.058	5.232	265.140	1.778	1.616	7.995
FRO 362A	440.73	7.366*E*-08	1.698	88.726	0.842	0.223	7.935	0.149	12.344	322.654	5.943	0.789	13.399
FRO 368A	447.90	1.210*E*-07	0.419	96.529	0.354	0.043	2.023	0.063	4.621	272.730	3.880	3.175	7.899
FRO 375	450.74	1.095*E*-07	1.673	87.261	1.274	0.191	6.922	0.138	10.958	340.317	2.883	2.578	12.987
FRO 400	461.18	6.602*E*-08	3.394	80.233	1.993	0.440	11.735	0.237	20.078	328.726	0.176	0.901	26.020

difference in χ behavior for each carbonate platform model. In this study, a homoclinal ramp and a rimmed shelf models have been investigated and they both show significant variation of the average χ values with the depositional settings (**Figures 5C,D**).

In the ramp model, χ values decrease toward- the shallowest facies. The χ general behavior coincides with previously published models (Mabille and Boulvain, 2007; Mabille et al., 2008a) for the Devonian ramps in south-western Belgium, corresponding to an increase of the average χ values along a proximal – distal profile. The high value for the RP-FF1 facies is explained by the higher detrital content observed in this facies.

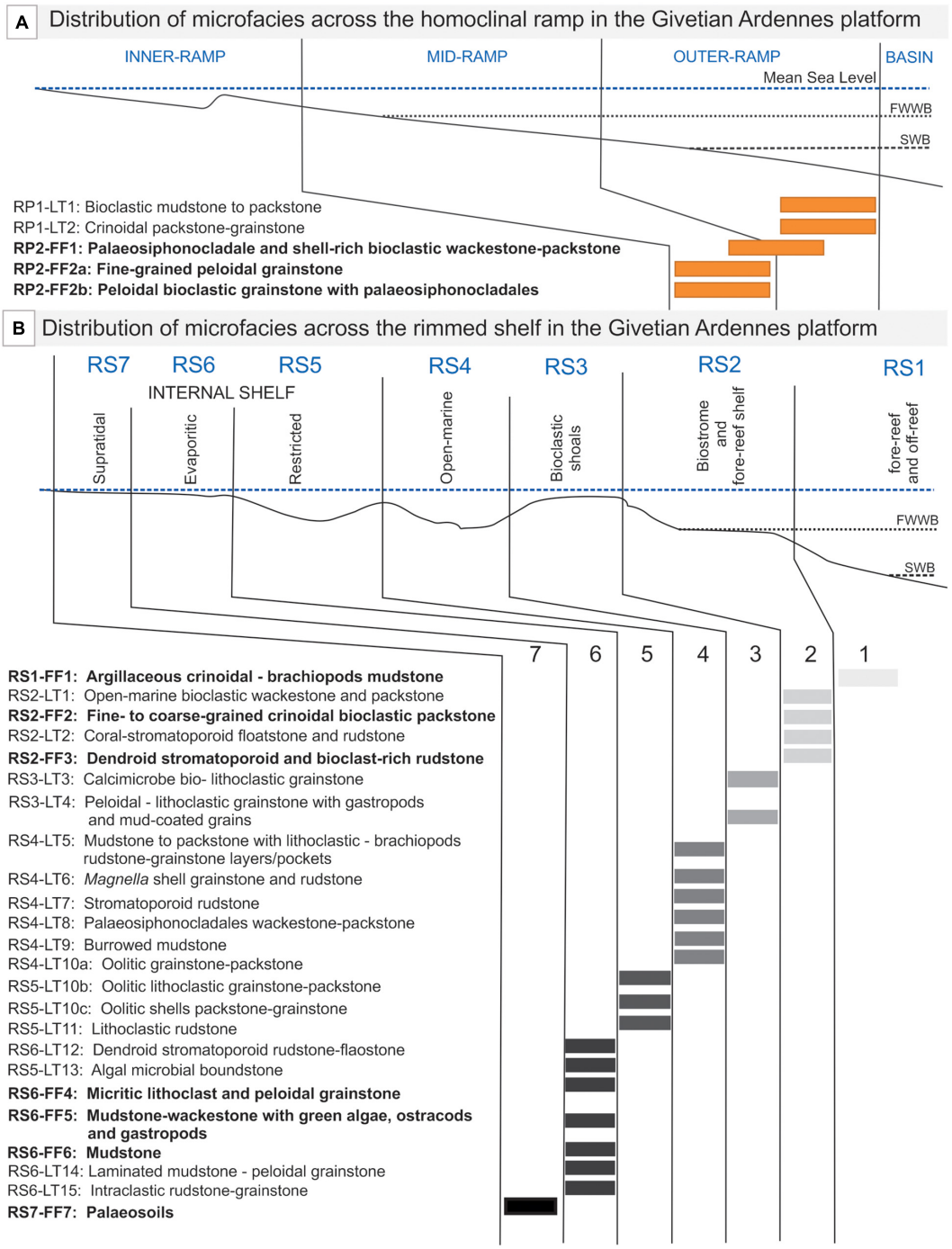

FIGURE 7 | Distribution and name of microfacies across the different sedimentological models based on the combination of this study and published results by Pas et al. (2017). Microfacies in bold are only observed in the FF section. **(A)** Distribution of microfacies along the homoclinal ramp. **(B)** Distribution of microfacies along the rimmed shelf profile. The fair-weather wave base (FWWB) and storm wave base (SWB) are presented for each model.

In the rimmed shelf model, the general decrease of the average χ signal from the off-reef to biostromal belts that characterize the external belt is similar to observations reported in Da Silva et al. (2009) for similar external shelf setting in Belgian Frasnian successions. This decrease is explained by an increase of both carbonate productivity and hydro-energy, which either trigger a dilution of the χ carrying particles and/or prevent them to settle down. The decrease of the average χ value toward the oolitic shoal is assumed to be driven by the high hydro-energy characterizing shoals in shelf interior, preventing

χ carrying minerals from settling down. The higher average χ value for the RS7 is explained by the vicinity of this belt with the emerged landmass and the potential influence of paleosoil development (i.e., ferro-siderite precipitation) and therefore a direct and higher influence of riverine and eolian input. The syn-sedimentary processes and carbonate productivity are commonly involved to explain model of χ variations along a distal proximal transect (Da Silva et al., 2013). The χ varying behavior in the internal and external shelf settings is also clearly visible on the χ curves constructed for the FF section (**Figure 2**), where each deepening upward in microfacies is characterized by increasing χ values. Variation of χ as a function of depositional setting also strongly advocates for preservation of the depositionally-induced trends in the χ signal despite the remagnetization affecting the area. Another example supporting the preservation of the χ signal is the observation of an astronomically-forced imprint in both sections (De Vleeschouwer et al., 2015). These astronomical imprints were used to build an astronomically-tuned time scale for the Givetian Stage.

In summary, the comparison of the χ signal with detrital and depositional proxies has revealed that the recorded χ in the LT and FF sections is still carrying a well-preserved primary signal despite the remagnetized fingerprint established through the analysis of hysteresis parameters. The χ signal in FF and LT sections thus corresponds to the superposition of a primary depositional χ signal overprinted by the χ carried by the secondary diagenetic magnetic minerals likely related to the C-component of Zegers et al.'s (2003) remagnetization event. The preservation of the χ signal in LT and FF sections indicates that the C-component with formation of fine-grained ferromagnetic minerals did not strongly affect or distort the primary χ trends. The C-component is interpreted as formed during the smectite to illite transition, a process that does not require external fluids in the system to be important (Zegers et al., 2003). As suggested by Da Silva et al. (2012) for Devonian carbonate in Belgium, we propose that during the formation of the secondary diagenetic fine-grained magnetic fingerprint in LT and FF sediments the system remained in situ or isochemical, so the authigenic-related susceptibility minerals did not strongly affect the primary signal and even enhanced it.

Early-Late Givetian Sea-Level Fluctuations and Carbonate Platform Development

When we compare the microfacies and magnetic susceptibility evolution for the Givetian sequences in Belgium and France, parallel trends occur in time-equivalent deposits (**Figure 8**) although both areas are separated by nearly a 100 km. The similarities in χ and microfacies patterns agree with published data (Boulvain and Préat, 1986; Préat et al., 1987; Préat and Boulvain, 1988; Bultynck et al., 1991; Boulvain et al., 1995; Préat, 2006; Préat and Bultynck, 2006; Boulvain et al., 2009; Maillet et al., 2011; Maillet et al., 2013) and allowed us to correlate a series of sedimentological events between the southern and the western margin of the Ardennes Givetian platform. In addition, the correlation of shallowing and deepening trends confirmed the occurrence of barrier-reefs through the Middle-Late Givetian within the intermediate buried part of the platform and completed the stratigraphic and paleogeographic model proposed in Figure 23 in Boulvain et al. (2009) (**Figure 9**). It is important to note that labels referred in Pas et al. (2017) that defined the main sedimentary interval and MSU (e.g., I to V, MSUI-V) had to be modified to create a comprehensive correlation chart included both stratigraphic records. Interval I (MSU-I) in Pas et al. (2017) became interval III (MSU-II) in this study and the same modification applies for all the sedimentary intervals.

Figure 8 shows the correlation between the main depositional changes (intervals I to VII) and the associated shallowing – deepening trends interpreted for the Givetian in the Ardennes.

The first depositional interval (I) within the Lower Givetian was deposited within the storm wave base (SWB) on a homoclinal ramp. Deposition on a ramp is unusual for this time in the southern margin of the Ardennes area. Indeed, classical sections (i.e., Glageon, Resteigne, Baileux; see location on **Figure 1B**) expose meter thick accumulations of reefal carbonate rich in stromatoporoids, corals, and algae, corresponding to the so-called "premier biostrome" (Préat et al., 1984). This "premier biostrome" is interpreted as the result of a reef that extends over 150 km, from Glageon in the west to Ferrieres in the east (Boulvain et al., 2009). The absence of reef-building organisms within the FF section suggests local changes in the environmental conditions, hampering reef-related deposition and creating a discontinuity in the reef. Time-equivalent shallow-water carbonate deposits located in the "Marenne Est" quarry section (Mabille et al., 2008a) (south-eastern part of the DS; located in **Figure 1B**) expose limestone with high concentration of sandy and silt materials. According to De Wilde (2005), the siliciclastic materials in the limestone are related to the Caledonian Stavelot Massif, which prompted increasing detrital inputs seaward, and thus inhibited the development of shallow-water communities. Another hypothesis explaining the absence of the "premier biostrome" in Fromelennes-Flohimont depositional area is that it was located in a fore-reef setting, south of the barrier-reef that had formed the "premier biostrome" (see Figure 16 in Boulvain et al., 2009).

The transition from the first (I) to the second (II) interval is characterized by an important change in microfacies, corresponding to the first occurrence of sediments interpreted as deposited in restricted lagoonal and supratidal settings (RS6 and RS7). This abrupt change in the sedimentary record is interpreted as a major sea-level fall, likely corresponding to the upper part of cycle If of Johnson et al. (1985). This event triggered basinward drift of adjacent reef-building communities, enabling the formation of a continuous "barrier" or paleo-high structures within the early Givetian. Indeed, we assume that during the sea-level fall reef-building communities, observed in interval (I) in adjacent areas, migrated basinward to accommodate the drop in the sea-level and rebuilt new reefal structures. As stated in Boulvain et al. (2009), the development of a reefal structure basinward (e.g., southward) is likely responsible for the lagoonal deposits occurring in the interval (II). Shoals structure could also be responsible for the development of landward lagoonal

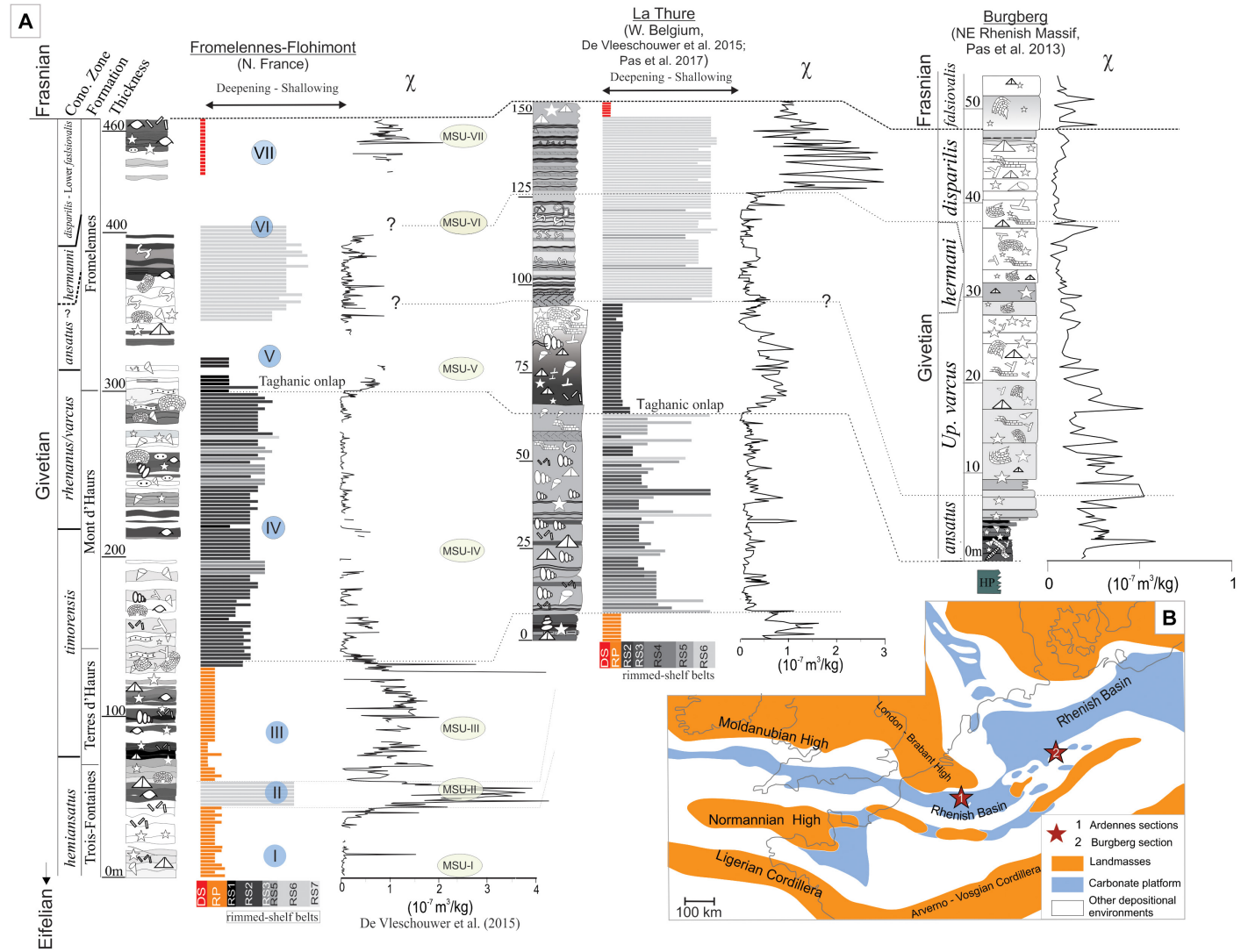

FIGURE 8 | Comparison and correlation of vertical microfacies evolution and associated magnetic susceptibility curves for the studied sections (Pas et al., 2013; De Vleeschouwer et al., 2015; Pas et al., 2017). Note that sedimentary intervals and MSU (e.g., I to V, MSUI-V) labels, as referred in Pas et al. (2017), had to be modified in order to build this correlation chart. For instance, interval I (MSU-I) in Pas et al. (2017) became interval III (MSU-II) in this study and the same modification applies for all defined sedimentary intervals. **(A)** Correlation chart showing the Ardennes and the Burgberg sections. Note that the scale of the χ values for the Burgberg section is not similar to those of the FF and LT sections in order to overcome the very low χ values in this section. **(B)** Middle Devonian paleogeographic setting showing the large carbonate platform developed in northern Europe and the relative location of the three sections, modified after Ziegler (1982) and McKerrow and Scotese (1990).

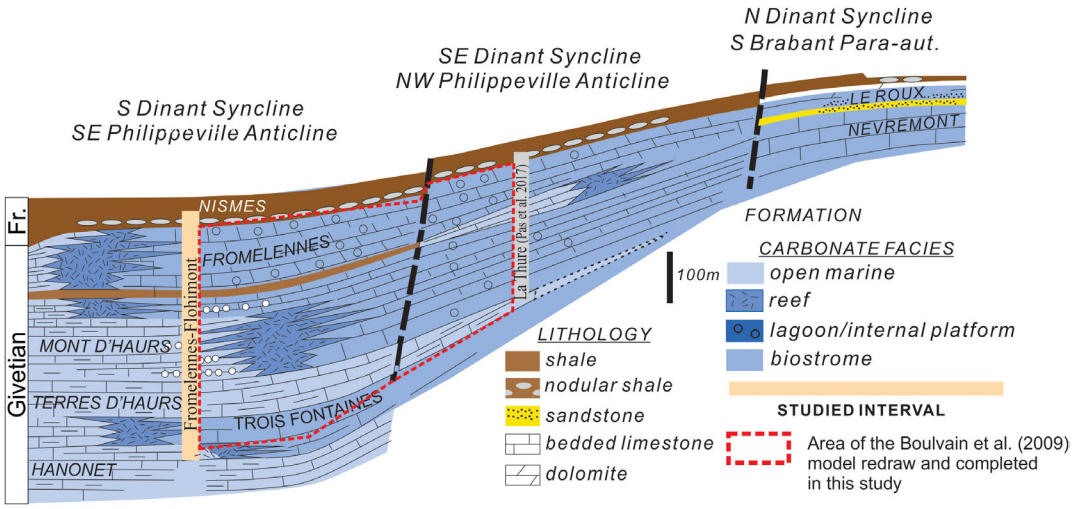

FIGURE 9 | Redraw and completed (red dotted line area) lithostratigrahic and paleogeographic framework for the Givetian in Belgium and France from Boulvain et al. (2009) showing the location of the new data collected in this study.

environments as they could produce wave attenuation. Assuming the thickness of carbonate (several tens of meters) characterizing this specific environment in the FF section, and in other locations in the south of the Ardennes (i.e., Resteigne, Marenne, Glageon), the reefal or paleo-high like shoal structures separating internal and external shelf should have been continuous and stable for a relatively long period of time. Given the lack of outcrops, the "barrier" or paleo-high controlling the lagoon development has never been observed. Although, we might assume that this "barrier" or paleo-high was located a few kilometers south of the Dinant Syncline southern margin. The E-W lateral extension of the "barrier" controlling the deposition of lagoonal sedimentation in the upper part of the Trois-Fontaine Fm. is illustrated in Figure 16 in Boulvain et al. (2009).

The transition to the third (III) Interval (e.g., Trois-Fontaine Fm. to Terre d'Haurs Fm., transition *hemiansatus* to *timorensis* conodont Zones), records a deepening trend and the return to a ramp model (RP). The homogenous deposits occurring throughout this third interval (III) are assumed to reflect a mid- to distal ramp environment influenced by storms, showing the local development of patch-reefs seen in outcrop. The similar evolution of microfacies and magnetic susceptibility in the uppermost part of the third interval (III) in FF section and the lowermost part of the LT section allowed us to match both sequences.

A principal turning point in facies and magnetic susceptibility occurs at the transition to the fourth (IV) interval, corresponding to a major sedimentological shift in the Ardennes. This transition from Interval (III) to (IV) is characterized in the south (Fromelennes-Flohimont), by a transition from mid- and outer-ramp settings (RP2-FF1) to biostromal and fore-reef shelf facies (RS2, open-marine deposits rich in reefal debris) with meters thick accumulation of reefal limestone while in the west (La Thure), the coeval transition consists of a change from mid-ramp (RP1-LT2) to well-bedded internal shelf deposits (RS3, RS4 and RS5). Such a contrast in facies must involve an important difference in paleo-depth and likely the existence of a reefal structures between both localities, supplying reefal debris basinward (e.g., biostromal and fore-reef shelf facies, RS2, see **Figure 2B** (pictures e-d)) and allowing an internal-shelf sedimentation landward (RS2, RS3, and RS5). Paleo-high structure such as shoals have not been proposed here because biostromal and fore-reef shelf facies observed in FF could not be derived from it. As a result of the Variscan folding in the area, this structure does not outcrop but must be located somewhere in the subsurface near the Dinant Syncline axis.

The transition to the fifth (V) interval is characterized by a major rise in sea-level, leading to the accumulation of off-reef and fore-reef deposits (RS1-FF1) in the FF section and biostromal and fore-reef facies (RS2-LT2-3) in the LT section. As discussed in Pas et al. (2017), this sea-level increase was associated with the so-called Taghanic Onlap (Johnson, 1970) (event IIa in Johnson et al., 1985) which led to major extinctions within a number of groups in both the marine and terrestrial realm (Aboussalam and Becker, 2011; Marshall et al., 2011).

Shortly after this major sea-level rise, both sections record a shallowing-upward shift defining the intervals (V) and (VI) transition. This sea-level drop corresponds to a similar shift of facies from fore-reef (RS1 and RS2) to internal shelf (RS5, RS4) in both sections. The causes of this particular transition to very shallow settings is explained in Pas et al. (2017).

The transition to Interval (VII) is marked by the drowning of the lagoonal deposits (e.g., RP-LT1) in both areas. Densely-packed brachiopod-bivalves shell levels forming these drowning deposits are several tens of meters thick in FF but only several meters thick in the LT section (see Figure 3 in Pas et al., 2017). As summarized in Pas et al. (2017), the drowning of the Ardennes Givetian platform could be triggered by the combination of the

global late Devonian sea-level rise, the increasing terrestrial influx and the active syn-sedimentary faulting.

Reliability of χ Records for Long-Distance Correlation of Million-Year Trends in Devonian Carbonate: Implication for the Devonian Stratigraphy

Belgian and France long-term χ curves and sedimentological patterns can be easily correlated (**Figure 8**) despite (1) the Late Variscan remagnetization event recognized by Zegers et al. (2003), (2) the hundred kilometers separating both localities and (3) the different depositional background. In the Ardennes, the similarity in the χ evolution model through a proximal – distal transect ranging from south to north can be partly attributed to a similar response of the environment to external environmental forcing (e.g., relative sea-level variations and siliciclastic influx change). On an intra-basinal/regional scale, the magnetic susceptibility tool has already been successfully used for the correlation of sections (Whalen and Day, 2010; Da Silva and Boulvain, 2012). An important question that arises from these results is if the million year scale correlations of χ records are reliable on a larger inter-regional scale. The χ signal as a tool for inter-regional correlation of stratigraphic records has already been assessed by different authors (e.g.,Ellwood et al., 1999; Ellwood et al., 2001, 2008; Boulvain et al., 2010). Their results suggested the high potential of χ signal for global correlation in ancient sedimentary sequences. Whereas promising, these results lack the geochemical and magnetic basis that are now regarded as crucial prior to any interpretation or use of the χ signal (e.g., Da Silva et al., 2015).

Using available conodont data, marker beds (e.g., Taghanic onlap) and the sedimentological patterns, we have developed a correlation chart (**Figure 8A**) comparing Givetian datasets from the Ardennes with the time-equivalent data from the Burgberg section in Germany (Pas et al., 2013). These sites bordered the Old Red continent in the north (see **Figure 8B**) and were located at the same paleolatitude, near the equator (see Figure 7 in Eckelmann et al., 2014). At present, the Burgberg area is situated ∼280 km away from the FF section and ∼340 km from the LT section (see **Figure 1A**). Assuming a Variscan compression with a NE-SW direction and the fact that the Burgberg section is located in the northeast of the Ardennes, we made the assumption that the distance between LT and Burgberg, and FF and Burgberg should not be that much different than today. Finally, the Burgberg section corresponds to a fore-reef related deposition providing a good biostratigraphic constraint. In addition, the results from the magnetic susceptibility, the sedimentological observations, the geochemistry and magnetic hysteresis measurements indicated a well-preserved χ signal (Pas et al., 2013; Pas, 2015).

Published χ records from time-equivalent sections in United States, Czech Republic, and Morocco (Ellwood et al., 1999, 2011; Hladil et al., 2006) have not been used for comparison in the following discussion because the preservation of χ signal was not established through geochemistry or hysteresis measurements. Indeed, an important aspect of this assessment is to compare datasets which show a preserved χ signal.

Visual evaluation of the long-term χ trends recorded from the Ardennes and the Burgberg sections highlight a lack of correlation, e.g., the χ signal increase just prior the Givetian-Frasnian boundary in Belgium and France but a reverse trend is observed in Germany. Another well-visible example occurs in the *disparilis* – Lower *falsiovalis* zone where χ signal shows high and strongly fluctuating values in Belgium but very stable low values in Germany.

The first element that might have influenced the lack of correlation between the Ardennes and the Burgberg sections is the sampling resolution of our χ records, as well as the resolution of the conodont zonation. Indeed, in thick shallow-water successions such as the FF and LT sections, the biostratigraphic constraint is relatively weak compared to the Burgberg section, which is well-constrained by conodonts. Moreover the average sampling interval for all the sections is the same, whereas the sections have different sedimentation rates. For instance, for the Givetian interval in the relatively condensed Burgberg section, we collected around 200 samples while in the FF section for slightly shorter time-scale we count nearly 600 samples. This difference in the relative sampling interval has a direct impact on the χ signal resolution and may reduce the visibility of the expected long-term trends but it should not modify the main trends observed throughout the sections.

Another major element that should be considered in understanding the different pattern in χ trends between the LT, FF and Burgberg sections is the impact of the various depositional parameters on the χ signal recorded over short- and long-time scales in marine sedimentary rocks. They are depositional variations that arise due to factors inherent to the sedimentary system (i.e., autogenic; wave agitation, lateral migration of sediment body, tidal current, channel migration, paleosoil development) and to externally controlled forcing such as climate, tectonic, source rocks and sea-level/accommodation (i.e., allogenic).

Allogenic parameters are acting over both, long- and short-time scales and are the primary causes of changes in detrital supply basinward, which is itself the strongest χ primary-controlling factor (e.g., Crick et al., 1997; Vanderaveroet et al., 1999; Ellwood et al., 2000; Śliwiński et al., 2012). Autogenic processes play a role over small spatial and temporal scales and they have the potential to remove all evidence from sedimentary archives that originated from low-magnitude or high-frequency climate or tectonic changes (Jerolmack and Paola, 2010). Shallow carbonate platforms such as the one under investigation here commonly exhibit a pronounced lateral heterogeneity where coral reefs, oolitic or bioclastic shoals, lagoons, and tidal flats are juxtaposed (facies mosaic; Wright and Burgess, 2005) and therefore such context is particularly influenced by autogenic processes.

For each section investigated in this study we explored the link between average χ signal and syn-sedimentary parameters such as wave agitation, carbonate productivity/sedimentation rate and the vicinity to landmasses through the qualitative

comparison with facies belts/microfacies (see section Magnetic Susceptibility versus Detrital and Depositional Proxies and **Figures 5C,D**). Across different platform profiles, the impact of syn-sedimentary processes were proven to exert a significant role in the χ signature (e.g., Bábek et al., 2007; Mabille et al., 2008b; Da Silva et al., 2009). Concerning the Givetian sections in Ardennes two models of magnetic susceptibility evolution were considered (e.g., homoclinal ramp and rimmed shelf; **Figures 5C,D**). For the Burgberg section, deposited in a fore-reef setting, the model shows χ values decreasing through shallowing upward facies (Pas, 2015; p. 57), which is hence a completely different χ evolutionary model than those highlighted in Ardennes sections. For instance, weak current and wave agitation (e.g., off-reef setting) will allow magnetic particles to settle down and concentrate in the sediment, while substantial wave agitation (e.g., barrier or shoals settings) will prevent the settlement of small particles carrying the magnetic susceptibility (see Da Silva et al., 2009 for an overview of the influence of local environmental parameters on the magnetic susceptibility). In other words, we suggest that autogenic processes, which operate at small spatial and temporal scales and modulate the externally-forced χ signal have a strong influence over the final magnetic susceptibility signal. This influence varies from one depositional locality to another due to the various sedimentary processes, and can result in the absence of correlation in the long-term χ signal. On a regional scale and for a shorter time-interval (e.g., three to four conodont Zones), Da Silva et al. (2009) observed a similar pattern when trying to correlate time-equivalent χ curves obtained in the distal and the intermediate part of the Belgian Frasnian platform; distal and intermediate (internal) part are ruled by different χ evolutionary models.

Long-distance χ based correlations in remagnetized settings must be considered carefully because the situation is more complex, and time-equivalent long-term χ curves from other paleogeographic settings and platforms are still highly necessary. Magnetic susceptibility-based correlation from modern deep-sea and other deep marine repositories (Ridgwell, 2002; Irino and Tada, 2003; Larrasoaña et al., 2008; Weber et al., 2012) showed spectacular results which are recommended for performing long-distance correlation. Deep-marine records are much less affected by syn-sedimentary processes and have proven to carry a more complete signal. This because they are less subject to severe alteration by chemical and physical processes as well as erosion/redeposition, as observed in continental or shallow-marine deposits.

CONCLUSION

The Fromelennes-Flohimont section is composed of a large number of microfacies organized in three sedimentological models, a rimmed shelf, a homoclinal ramp and a drowning shelf. The early Givetian homoclinal ramp evolved to a rimmed shelf throughout middle- to late-Givetian, and by the latest Givetian the platform drowned, and was subsequently capped by Frasnian shales.

Hysteresis measurements on our sample sets indicate a χ signal predominantly controlled by ferromagnetic (s.l.) minerals although paramagnetic and diamagnetic minerals such as clay, pyrite and calcite, also contributed to χ. Low-coercivity ferromagnetic component ($H_{cr} < 60$ mT), such as magnetite have the strongest influence on χ variations within the sampled sections. Even though the high-coercivity minerals, such as hematite, are clearly indicated in both sections, their influence on the χ is weak. The analysis of H_{cr}/H_c and M_{rs}/M_s ratios on samples with an $IRM_{300}/IRM_{500} < 5\%$ indicates a χ signal distinctly influenced by fine-grained SP magnetic particles, which are also shown through the analysis of S_d values. These SP grains have probably been formed during the Carboniferous remagnetization in the Ardennes. Nevertheless, the comparison of χ with facies evolution and terrestrial proxies clearly shows that the χ in both datasets is carrying primary depositional signal. The χ signal in FF and LT sections result from a primary depositional χ signal overprinted by the susceptibility carried by the secondary diagenetic magnetic minerals. The secondary diagenetic overprint did not obliterated the primary signal, hence, it can potentially be used as for correlation and paleoenvironmental interpretation.

Comparison of long-time scale sedimentological and χ profiles of time-equivalent sequences from Belgium and France emphasized similarities despite the different sedimentological background, the remagnetization affecting the region and the relatively long-distance separating the sections. This regional correlation provided new information allowing us to recognize important sedimentary changes during the Givetian in the Ardennes, some of them correlated with major Devonian T-R events (e.g., T-R IIa or Taghanic Event).

The correlation of depositional trends between the southern and the western margin of the platform confirmed the occurrence of barrier-reefs through the Middle-Late Givetian within the intermediate buried part of the platform and to complete the previously published stratigraphic and paleogeographic model.

The Belgian/French sections were compared with the Burgberg section in Germany using the magnetic susceptibility signal, but the correlations are not successful.

Our analyses show that similar facies development along a carbonate platform profile, in response to changes caused by sea-level fluctuations, might result in a similar model of χ profiles that can be used for correlation. We also suggested that the different modulation of the long-term changes in the allogenic χ signal by autogenic processes could be responsible for the absence of correlation between the long-term χ curves in Ardennes and the Rheinisches Schiefergebirge.

DATA AVAILABILITY STATEMENT

Publicly available datasets were analyzed in this study. This data can be found here: https://doi.org/10.1594/PANGAEA.855764. All additional raw data supporting the conclusion of this article will be made available by the author, without due reservation, to any qualified researcher.

AUTHOR CONTRIBUTIONS

DP conceived the study, carried out the research, and wrote the manuscript. A-CD and FB contributed to the interpretation and discussion. GP collected the rock samples. SS provided access to the hysteresis measurement device and helped at interpreting the dataset.

ACKNOWLEDGMENTS

This work was partly written during a post-doctoral fellowship awarded by a BeIPD Marie-Curie COFUND Program (University of Liège, Belgium) assigned to DP (Grant N° 600405). A-CD and DP acknowledge the Netherlands Organization for Scientific Research (NWO, grant WE.210012.1). We are very grateful to Sean Karoly of George Mason University (United States) for his thorough review of the English. We would like to thank the editor KK and the two reviewers for their constructive comments that helps at improving the quality of this manuscript. We would also like to express our thanks to Michael Whalen, John. J. G. Reijmer, Peir Pufahl, Erika Kido, and Marco Maffione who contributed to improve previous versions of this manuscript. This paper is a contribution of the IGCP-652 project "Reading geologic time in Paleozoic sedimentary rocks: the need for an integrated stratigraphy."

SUPPLEMENTARY MATERIAL

The Supplementary Material for this article can be found online at: https://www.frontiersin.org/articles/10.3389/feart.2019.00341/full#supplementary-material

REFERENCES

Aboussalam, Z. S., and Becker, R. T. (2011). The global Taghanic Biocrisis (Givetian) in the eastern Anti-Atlas, Morocco. *Palaeogeogr. Palaeoclimatol. Palaeoecol.* 304, 136–164. doi: 10.1016/j.palaeo.2010.10.015

Bábek, O., Pøikryl, T., and Hladil, J. (2007). Progressive drowning of carbonate platform in the Moravo-Silesian Basin (Czech Republic) before the Frasnian/Famennian event: facies, compositional variations and gamma-ray spectrometry. *Facies* 53, 293–316. doi: 10.1007/s10347-006-0095-8

Belanger, I., Delaby, S., Delcambre, B., Ghysel, P., Hennebert, M., Laloux, M., et al. (2012). Redéfinition des unités structurales du front varisque utilisées dans le cadre de la nouvelle Carte géologique de Wallonie (Belgique). *Geol. Belg.* 15, 169–175.

Borradaile, G. J., Chow, N., and Werner, T. (1993). Magnetic hysteresis of limestones: facies control? *Phys. Earth Planet. Inter.* 76, 241–252. doi: 10.1016/0031-9201(93)90016-3

Boulvain, F., Coen-Aubert, M., Mansy, J. L., Proust, J. N., and Tourneur, F. (1995). Le Givetien en Avesnois (Nord de la France): paléoenvironnements et implications paléogéographiques. *Bull. de la Société belge de Géol.* 103, 171–203.

Boulvain, F., Da Silva, A. C., Mabille, C., Hladil, J., Gersl, M., Koptikova, L., et al. (2010). Magnetic susceptibility correlation of km-thick Eifelian-Frasnian sections (Ardennes and Moravia). *Geol. Belg.* 13, 309–318.

Boulvain, F., Mabille, C., Poulain, G., and Da Silva, A. C. (2009). Towards a palaeogeographical and sequential framework for the givetian of Belgium. *Geol. Belg.* 12, 161–178.

Boulvain, F., and Préat, A. (1986). Les calcaires laminaires du Givétien Supérieur du bord sud du Bassin de Dinant (Belgique, France): témoins d'une évolution paléoclimatique. *Annales de la Societé Géologique de Belgique* 109, 609–619.

Bultynck, P. (1974). Conodontes de la formation de Fromelennes du Givetien de l'Ardenne franco-belge. *Bulletin de l'Institut Royal des Sciences Naturelles de Belgique Sciences de la Terre* 50, 1–30.

Bultynck, P. (1987). Pelagic and neritic conodont successions from the Givetian of pre-Sahara Morocco and the Ardennes. *Bulletin de l'Institut Royal des Sciences Naturelles de Belgique Sciences de la Terre* 57, 149–181.

Bultynck, P., Coen-Aubert, M., Dejonghe, L., Godefroid, J., Hance, L., Lacroix, D., et al. (1991). Les formations du Dévonien moyen de la Belgique. *Mémoires pour servir à l'explication des cartes géologiques et minières de la Belgique* 30, 1–105.

Bultynck, P., and Dejonghe, L. (2001). "Devonian lithostratigraphic units (Belgium)," in *Guide to a Revised Lithostratigraphic Scale of Belgium*, eds P. Bultynck, and L. Dejonghe, (Brussels: Geologica Belgica), 39–69.

Burov, B., Nurgaliev, D. K., and Jasonov, P. G. (1986). *Paleomagnetic Analysis Kazan*. Kazan: University Press.

Calvert, S. E., and Pedersen, T. F. (2007). "Chapter Fourteen Elemental Proxies for Palaeoclimatic and Palaeoceanographic Variability in Marine Sediments: Interpretation and Application," in *Developments in Marine Geology*, eds H. M. Claude, and D. V. Anne, (Amsterdam: Elsevier), 567–644. doi: 10.1016/s1572-5480(07)01019-6

Chadimova, L., Vacek, F., Sobien, K., Slavik, L., and Hladil, J. (2015). Petrophysical record of the Late Silurian shallow-water carbonate facies across the Lau Event (Prague Synform, Czech Republic) and dynamic time warping alignment of the magnetic susceptibility logs. *Geol. Soc. Spec. Publ.* 414, 133–155. doi: 10.1144/SP414.14

Channell, J. E. T., and McCabe, C. (1994). Comparison of magnetic hysteresis parameters of unremagnetized and remagnetized limestones. *J. Geophys. Res.* 99, 4613–4623. doi: 10.1029/93jb02578

Crick, R. E., Ellwood, B. B., El Hassani, A., Feist, R., and Hladil, J. (1997). Magnetosusceptibility event and cyclostratigraphy (MSEC) of Eifelian-Givetian GSSP and associated boundary sequences in North Africa and Europe. *Episodes* 20, 167–175. doi: 10.18814/epiiugs/1997/v20i3/004

Da Silva, A. C., and Boulvain, F. (2012). Analysis of the Devonian (Frasnian) platform from Belgium: a multi-faceted approach for basin evolution reconstruction. *Basin Res.* 24, 338–356. doi: 10.1111/j.1365-2117.2011.00526.x

Da Silva, A. C., De Vleeschouwer, D., Boulvain, F., Claeys, P., Fagel, N., Humblet, M., et al. (2013). Magnetic susceptibility as a high-resolution correlation tool and as a climatic proxy in Paleozoic rocks - Merits and pitfalls: examples from the Devonian in Belgium. *Mar. Pet. Geol.* 46, 173–189. doi: 10.1016/j.marpetgeo.2013.06.012

Da Silva, A. C., Dekkers, M. J., Mabille, C., and Boulvain, F. (2012). Magnetic susceptibility and its relationship with paleoenvironments, diagenesis and remagnetization: examples from the Devonian carbonates of Belgium. *Stud. Geophys. Geod.* 56, 677–704. doi: 10.1007/s11200-011-9005-9

Da Silva, A. C., Mabille, C., and Boulvain, F. (2009). Influence of sedimentary setting on the use of magnetic susceptibility: examples from the Devonian of Belgium. *Sedimentology* 56, 1292–1306. doi: 10.1111/j.1365-3091.2008.01034.x

Da Silva, A. C., Whalen, M. T., Hladil, J., Chadimova, L., Chen, D., Spassov, S., et al. (2015). Magnetic susceptibility application: a window onto ancient environments and climatic variations. *Geol. Soc. Lond. Spec. Pub.* 414:283. doi: 10.1144/sp414.12

Day, R., Fuller, M., and Schmidt, V. A. (1977). Hysteresis properties of titanomagnetites: grain-size and compositional dependence. *Phys. Earth Planet. Inter.* 13, 260–267. doi: 10.1016/0031-9201(77)90108-X

De Vleeschouwer, D., Boulvain, F., Da Silva, A.-C., Pas, D., Labaye, C., and Claeys, P. (2015). The astronomical calibration of the Givetian (Middle Devonian) timescale (Dinant Synclinorium, Belgium). *Geol. Soc. Lond. Spec. Pub.* 414, 245–256. doi: 10.1144/sp414.3

De Wilde, C. (2005). *Sédimentologie de la Formation de Trois-Fontaines à Marenne*. Msc thesis, Université de Liège, Liège

Devleeschouwer, X., Petitclerc, E., Spassov, S., and Préat, A. (2010). The Givetian-Frasnian boundary at nismes parastratotype (Belgium): the magnetic susceptibility signal controlled by ferromagnetic minerals. *Geol. Belg.* 13, 351–366.

Dittmar, D., Meyer, W., Oncken, O., Schievenbusch, T., and Von Winterfeld, C. (1994). Strain partitioning across a fold and thrust belt, the Rhenish Massif, Mid)European Variscides. *J. Struct. Geol.* 16, 1335–1352. doi: 10.1016/0191-8141(94)90001-9

Dunlop, D. J. (2002). Theory and application of the Day plot (Mrs/Ms versus Hcr/Hc) 1. Theoretical curves and tests using titanomagnetite data. *J. Geophys. Res. Atmos.* 107, 260–267.

Eckelmann, K., Nesbor, H. D., Königshof, P., Linnemann, U., Hofmann, M., Lange, J. M., et al. (2014). Plate interactions of Laurussia and Gondwana during the formation of Pangaea - Constraints from U-Pb LA-SF-ICP-MS detrital zircon ages of Devonian and Early Carboniferous siliciclastics of the Rhenohercynian zone, Central European Variscides. *Gondwana Res.* 25, 1484–1500. doi: 10.1016/j.gr.2013.05.018

Ellwood, B. B., Crick, R. E., and El Hassani, A. (1999). Magnetosusceptibility event and cyclostratigraphy (MSEC) method used in geological correlation of Devonian rocks from Anti-Atlas Morocco. *Am. Assoc. Pet. Geol. Bull.* 83, 1119–1134.

Ellwood, B. B., Crick, R. E., Garcia-Alcalde Fernandez, J. L., Soto, F. M., Truyols-Massoni, M., El Hassani, A., et al. (2001). Global correlation using magnetic susceptibility data from Lower Devonian rocks. *Geology* 29, 583–586.

Ellwood, B. B., Crick, R. E., Hassani, A. E., Benoist, S. L., and Young, R. H. (2000). Magnetosusceptibility event and cyclostratigraphy method applied to marine rocks: detrital input versus carbonate productivity. *Geology* 28, 1135–1138. doi: 10.1130/0091-7613200028<1135:meacma<2.0.co;2

Ellwood, B. B., Tomkin, J. H., El Hassani, A., Bultynck, P., Brett, C. E., Schindler, E., et al. (2011). A climate-driven model and development of a floating point time scale for the entire Middle Devonian Givetian Stage: a test using magnetostratigraphy susceptibility as a climate proxy. *Palaeogeogr. Palaeoclimatol. Palaeoecol.* 304, 85–95. doi: 10.1016/j.palaeo.2010.10.014

Ellwood, B. B., Tomkin, J. H., Ratcliffe, K. T., Wright, M., and Kafafy, A. M. (2008). High-resolution magnetic susceptibility and geochemistry for the Cenomanian/Turonian boundary GSSP with correlation to time equivalent core. *Palaeogeogr. Palaeoclimatol. Palaeoecol.* 261, 105–126. doi: 10.1016/j.palaeo.2008.01.005

Elmore, R. D., London, D., Bagley, D., Fruit, D., and Gao, G. (1993). Remagnetization by basinal fluids: testing the hypothesis in the Viola Limestone, southern Oklahoma. *J. Geophys. Res.* 98, 6237–6254. doi: 10.1029/92jb02577

Gouwy, S., and Bultynck, P. (2003). Conodont based graphic correlation of the Middle Devonian formations of the Ardenne (Belgium): implications for stratigraphy and construction of a regional composite. *Rev. Española de Micropaleontol.* 35, 315–344.

Hladil, J., Gersl, M., Strnad, L., Frana, J., Langrova, A., and Spisiak, J. (2006). Stratigraphic variation of complex impurities in platform limestones and possible significance of atmospheric dust: a study with emphasis on gamma-ray spectrometry and magnetic susceptibility outcrop logging (Eifelian-Frasnian, Moravia, Czech Republic). *Int. J. Earth Sci.* 95, 703–723. doi: 10.1007/s00531-005-0052-8

Hladil, J., Slavik, L., Vondra, M., Koptikova, L., Cejchan, P., Schnabl, P., et al. (2011). Pragian-Emsian successions in Uzbekistan and Bohemia: magnetic susceptibility logs and their dynamic time warping alignment. *Stratigraphy* 8, 217–235.

Irino, T., and Tada, R. (2003). High-resolution reconstruction of variation in aeolian dust (Kosa) deposition at ODP site 797, the Japan Sea, during the last 200 ka. *Glob. Planet. Change* 35, 143–156. doi: 10.1016/S0921-8181(02)00135-2

Jackson, M. (1990). Diagenetic sources of stable remanence in remagnetized Paleozoic cratonic carbonates: a rock magnetic study. *J. Geophys. Res.* 95, 2753–2761.

Jerolmack, D. J., and Paola, C. (2010). Shredding of environmental signals by sediment transport. *Geophys. Res. Lett.* 37:L19401. doi: 10.1029/2010GL044638

Johnson, J. G. (1970). Taghanic onlap and the end of north american devonian provinciality. *Bull. Geol. Soc. Am.* 81, 2077–2106.

Johnson, J. G., Klapper, G., and Sandberg, C. A. (1985). Devonian eustatic fluctuations in Euramerica. *Geol. Soc. Am. Bull.* 96, 567–587.

Königshof, P., Da Silva, A. C., Suttner, T. J., Kido, E., Waters, J., Carmichael, S. K., et al. (2016). Shallow-water facies setting around the Kaèák event: a multidisciplinary approach. *Geol. Soc. Lond. Spec. Pub.* 423, 171–199. doi: 10.1144/sp423.4

Larrasoaña, J. C., Roberts, A. P., and Rohling, E. J. (2008). Magnetic susceptibility of eastern mediterranean marine sediments as a proxy for Saharan dust supply? *Mar. Geol.* 254, 224–229. doi: 10.1016/j.margeo.2008.06.003

Mabille, C., and Boulvain, F. (2007). Sedimentology and magnetic susceptibility of the Upper Eifelian-Lower Givetian (Middle Devonian) in SW Belgium: insights into carbonate platform initiation. *Geol. Soc. Spec. Publ.* 275, 109–123. doi: 10.1144/gsl.sp.2007.275.01.08

Mabille, C., De Wilde, C., Hubert, B., Boulvain, F., and Da Silva, A. C. (2008a). Detailed sedimentological study of a non-classical succession for Trois-Fontaines and Terres d'Haurs formations (Lower Givetian, Marenne, Belgium) - Introduction to the Marenne Member. *Geol. Belg.* 11, 217–238.

Mabille, C., Pas, D., Aretz, M., Boulvain, F., Schröder, S., and Silva, A. C. (2008b). Deposition within the vicinity of the Mid-Eifelian High: detailed sedimentological study and magnetic susceptibility of a mixed ramp-related system from the eifelian lauch and nohn formations (Devonian. Ohlesberg, Eifel, Germany). *Facies* 54, 597–612. doi: 10.1007/s10347-008-0145-5

Maillet, S., Milhau, B., and Dojen, C. (2013). Stratigraphical distribution of Givetian ostracods in the type-area of the Fromelennes Formation (Fromelennes, Ardennes, France) and their relationship to global event. *Bull. Geosci.* 88, 865–892. doi: 10.3140/bull.geosci.1424

Maillet, S., Milhau, B., and Pinte, E. (2011). The fromelennes formation in the type-area (Fromelennes, Ardennes, France). *Ann. de la Soc. Géol. du Nord* 18, 9–34.

Mansy, J. L., Lacquement, F., Meilliez, F., and Van Vliet-Lanoë, B. (2006). *Carte géologique de France (1/50000), feuille Givet (40),* 2nd Edn. Orléans: BRGM.

Marshall, J. E. A., Brown, J. F., and Astin, T. R. (2011). Recognising the Taghanic Crisis in the Devonian terrestrial environment and its implications for understanding land-sea interactions. *Palaeogeogr. Palaeoclimatol. Palaeoecol.* 304, 165–183. doi: 10.1016/j.palaeo.2010.10.016

McKerrow, W. S., and Scotese, C. R. (1990). *Paleozoic Palaeogeography and Biogeography*. London: The Geological Society.

Molina Garza, R. S., and Zijderveld, J. D. A. (1996). Paleomagnetism of Paleozoic strata, Brabant and Ardennes Massifs, Belgium: implications of prefolding and postfolding Late Carboniferous secondary magnetizations for European apparent polar wander. *J. Geophys. Res. B Solid Earth* 101, 15799–15818. doi: 10.1029/96jb00325

Narkiewicz, K., and Bultynck, P. (2010). The upper Givetian (Middle Devonian) Subterminus conodont zone in North America, Europe and North Africa. *J. Paleontol.* 84, 588–625. doi: 10.1666/10-029.1

Parry, L. G. (1982). Magnetization of immobilized particle dispersions with two distinct particle sizes. *Phys. Earth Planet. Inter.* 28, 230–241. doi: 10.1016/0031-9201(82)90004-8

Pas, D. (2015). *Sedimentary Development and Correlation of Long-Term Off-Reef to Shallow-Water Devonian Carbonate Records in Europe*. Ph.D. thesis, University of Liège, Liège.

Pas, D., Da Silva, A. C., Cornet, P., Bultynck, P., Königshof, P., and Boulvain, F. (2013). Sedimentary development of a continuous Middle Devonian to Mississippian section from the fore-reef fringe of the Brilon Reef Complex (Rheinisches Schiefergebirge, Germany). *Facies* 59, 969–990. doi: 10.1007/s10347-012-0351-z

Pas, D., Da Silva, A. C., Devleeschouwer, X., De Vleeschouwer, D., Cornet, P., Labaye, C., et al. (2017). Insights into a million-year-scale Rhenohercynian carbonate platform evolution through a multi-disciplinary approach: example of a Givetian carbonate record from Belgium. *Geol. Mag.* 154, 707–739. doi: 10.1017/S0016756816000261

Pas, D., Da Silva, A. C., Devleeschouwer, X., De Vleeschouwer, D., Labaye, C., Cornet, P., et al. (2015). Sedimentary development and magnetic susceptibility evolution of the Frasnian in Western Belgium (Dinant Synclinorium, La Thure section). *Geol. Soc. Lond. Spec. Pub.* 414, 15–36. doi: 10.1144/sp414.7

Préat, A. (2006). Le Givétien franco-belge: moteur de la sédimentation eustatisme vs subsidence? *Géologie de la France* 1-2, 45–51.

Préat, A., and Boulvain, F. (1988). "Middle and upper Devonian carbonate platform evolution in Dinant and Namur Basins (Belgium, France)," in *Proceedings of the Excursion A-1, IAS 9th European Regional Meeting: Excursion Guidebook*, Leuven, 1–25.

Préat, A., and Bultynck, P. (2006). "Givetian," in *Chronostratigraphic Units Named from Belgium*, eds P. Bultynck, and L. Dejonghe, (Brussels: Geologica Belgica), 9–18.

Préat, A., Ceuleneer, G., and Boulvain, F. (1987). Etude sédimentologique des calcaires du Givétien Inférieur d'Olloy-sur-Viroin (bord Sud du Bassin de Dinant, Belgique). *Ann. de la Soc. Géol. du Nord* 106, 251–265.

Préat, A., Coen-Aubert, M., Mamet, B., and Tourneur, F. (1984). Sédimentologie et paléoécologie de trois niveaux récifaux du Givetien inférieur de Resteigne (bord sud du Bassin de Dinant, Belgique). *Bull. de la Soc. belge de Géol.* 93, 227–240.

Read, J. F. (1985). Carbonate platform facies models. *Am. Assoc. Pet. Geol. Bull.* 69, 1–21. doi: 10.1126/sciadv.1602158

Ridgwell, A. J. (2002). Dust in the earth system: the biogeochemical linking of land, air and sea. *Philos. Trans. R. Soc. A Math. Phys. Eng. Sci.* 360, 2905–2924. doi: 10.1098/rsta.2002.1096

Riquier, L., Averbuch, O., Devleeschouwer, X., and Tribovillard, N. (2010). Diagenetic versus detrital origin of the magnetic susceptibility variations in some carbonate Frasnian-Famennian boundary sections from Northern Africa and Western Europe: Implications for paleoenvironmental reconstructions. *Int. J. Earth Sci.* 99, 57–73. doi: 10.1016/j.palaeo.2014.09.030

Roberts, A. P., Tauxe, L., Heslop, D., Zhao, X., and Jiang, Z. (2018). A critical appraisal of the "Day" diagram. *J. Geophys. Res. Solid Earth* 123, 2618–2644. doi: 10.1002/2017jb015247

Sardar Abadi, M., Da Silva, A.-C., Mossadegh, H., Spassov, S., and Boulvain, F. (2015). Lower carboniferous ramp sedimentation of the Central Alborz Basin, northern Iran: integrated sedimentological and rock–magnetic studies. *Geol. Soc. Lond. Spec. Pub.* 414, 73–91. doi: 10.1144/sp414.13

Śliwinski, M. G., Whalen, M. T., and Day, J. (2010). Comparison of magnetic susceptibility (MS) and other geochemical proxies from the Middle-Late Frasnian of the Canadian Rocky Mountains: implications for paleoenvironmental and paleoclimatic analyses and interpretations of the punctata Event. *Przeglad Geol.* 58, 1152–1160.

Śliwiński, M. G., Whalen, M. T., Meyer, F. J., and Majs, F. (2012). Constraining clastic input controls on magnetic susceptibility and trace element anomalies during the Late Devonian punctata Event in the Western Canada Sedimentary Basin. *Terra Nova* 24, 301–309. doi: 10.1111/j.1365-3121.2012.01063.x

Spassov, S., and Valet, J. P. (2012). Detrital magnetizations from redeposition experiments of different natural sediments. *Earth Planet. Sci. Lett.* 351-352, 147–157. doi: 10.1016/j.epsl.2012.07.016

Tauxe, L., Bertram, H. N., and Seberino, C. (2002). Physical interpretation of hysteresis loops: micromagnetic modeling of fine particle magnetite. *Geochem. Geophys. Geosyst.* 3:1055. doi: 10.1029/2001GC000241

Tribovillard, N., Algeo, T. J., Lyons, T., and Riboulleau, A. (2006). Trace metals as paleoredox and paleoproductivity proxies: an update. *Chem. Geol.* 232, 12–32. doi: 10.1016/j.chemgeo.2006.02.012

Vanderaveroet, P., Averbuch, O., Deconinck, J. F., and Chamley, H. (1999). A record of glacial/interglacial alternations in Pleistocene sediments off New Jersey expressed by clay mineral, grain-size and magnetic susceptibility data. *Mar. Geol.* 159, 79–92. doi: 10.1016/S0025-3227(98)00203-5

Walden, J., Oldfield, F., and Smith, J. (1999). *Environmental Magnetism: A Practical Guide*. London: Quaternary Research Association.

Weber, M. E., Kuhn, G., Sprenk, D., Rolf, C., Ohlwein, C., and Ricken, W. (2012). Dust transport from Patagonia to Antarctica - A new stratigraphic approach from the Scotia Sea and its implications for the last glacial cycle. *Quat. Sci. Rev.* 36, 177–188. doi: 10.1016/j.quascirev.2012.01.016

Wehrmann, A., Hertweck, G., Brocke, R., Jansen, U., Königshof, P., Plodowski, G., et al. (2005). Paleoenvironment of an Early Devonian land-sea transition: a case study from the southern margin of the old red continent (Mosel Valley, Germany). *Palaios* 20, 101–120. doi: 10.2110/palo.2003.p03-33

Whalen, M. T., and Day, J. E. (2008). Magnetic susceptibility, biostratigraphy, and sequence stratigraphy: insights into Devonian carbonate platform development and basin infilling, western Alberta, Canada. *Soc. Sediment. Geol.* 89, 291–314. doi: 10.2110/pec.08.89.0291

Whalen, M. T., and Day, J. E. (2010). Cross-basin variations in magnetic susceptibility influenced by changing sea level, paleogeography, and paleoclimate: upper Devonian, western Canada sedimentary basin. *J. Sediment. Res.* 80, 1109–1127. doi: 10.2110/jsr.2010.093

Wright, V. P., and Burgess, P. M. (2005). The carbonate factory continuum, facies mosaics and microfacies: an appraisal of some of the key concepts underpinning carbonate sedimentology. *Facies* 51, 17–23. doi: 10.1007/s10347-005-0049-6

Zegers, T. E., Dekkers, M. J., and Baily, S. (2003). Late carboniferous to Permian remagnetization of Devonian limestones in the Ardennes: Role of temperature, fluids, and deformation. *J. Geophys. Res.* 108, 5/1–5/19.

Ziegler, A. P. (1982). *Geological Atlas of Western and Central Europe*. Brussels: Shell Internationale Petroleum Maatschappij B.V, 130.

Zwing, A., Bachtadse, V., and Soffel, H. C. (2002). Late Carboniferous remagnetisation of Palaeozoic rocks in the NE Rhenish Massif, Germany. *Phys. Chem. Earth A* 27, 1179–1188. doi: 10.1016/S1474-7065(02)00128-6

Zwing, A., Matzka, J., Bachtadse, V., and Soffel, H. C. (2005). Rock magnetic properties of remagnetized Palaeozoic clastic and carbonate rocks from the NE Rhenish massif, Germany. *Geophys. J. Int.* 160, 477–486. doi: 10.1111/j.1365-246X.2004.02493.x

Conflict of Interest: GP is now employed by the company Geolys.

The remaining authors declare that the research was conducted in the absence of any commercial or financial relationships that could be construed as a potential conflict of interest.

The handling Editor declared a past co-authorship with one of the authors DP.